



HAL
open science

Quantum spectral analysis: frequency in time

Mario Mastriani

► **To cite this version:**

| Mario Mastriani. Quantum spectral analysis: frequency in time. 2018. hal-01655209v3

HAL Id: hal-01655209

<https://inria.hal.science/hal-01655209v3>

Preprint submitted on 26 Dec 2018

HAL is a multi-disciplinary open access archive for the deposit and dissemination of scientific research documents, whether they are published or not. The documents may come from teaching and research institutions in France or abroad, or from public or private research centers.

L'archive ouverte pluridisciplinaire **HAL**, est destinée au dépôt et à la diffusion de documents scientifiques de niveau recherche, publiés ou non, émanant des établissements d'enseignement et de recherche français ou étrangers, des laboratoires publics ou privés.

Quantum spectral analysis: frequency in time

Mario Mastriani

Unidad de Información Cuántica, FIUBA, 850 Paseo Colon Av., C1063ACV, CABA, Argentina

mmastri@fi.uba.ar

ABSTRACT A *quantum time-dependent spectrum analysis*, or simply, a *quantum spectral analysis* (QSA) is presented in this work based on Schrödinger equation, which is a partial differential equation that describes how the quantum state of a non-relativistic physical system changes with time. In the classic world, it is named *frequency in time* (FIT), which is presented here in opposition and as a complement of traditional spectral analysis frequency-dependent based on Fourier theory. Besides, FIT is a metric, which assesses the impact of the flanks of a signal on its frequency spectrum, which is not taken into account by Fourier theory, let alone in real time. Even more, and unlike all derived tools from Fourier Theory, (i.e., continuous, discrete, fast, short-time, fractional and quantum Fourier Transform, as well as, Gabor) FIT has the following advantages among many others: a) compact support with excellent energy output treatment, b) low computational cost, $O(N)$ for signals and $O(N^2)$ for images, c) does not have phase uncertainties (indeterminate phase for magnitude = 0) as Discrete and Fast Fourier Transform has (DFT, FFT, respectively). In fact, FIT constitutes one side of a triangle (which from now on is closed) which consists of the original signal in time, the spectral analysis based on Fourier Theory and FIT. Thus a toolbox is completed, which is essential for all applications of Digital Signal Processing (DSP) and Digital Image Processing (DIP); and, even, in the latter, FIT allows edge detection (which is called flank detection in case of signals), denoising, despeckling, compression, and superresolution of still images. Such applications will be extremely useful for signals, imagery and communication intelligence.

Keywords Digital Signal and Image Processing • Fourier Theory • Imagery Intelligence • Quantum Image Processing • Quantum Information Processing • Quantum Signal Processing • Schrödinger equation • Signals Intelligence • Spectral Analysis.

1 Introduction

The main concepts related to Quantum Information Processing (QIP) may be grouped in the next topics: quantum bit (qubit, which is the elemental quantum information unity), Bloch's Sphere (geometric environment for qubit representation), Hilbert's Space (which generalizes the notion of Euclidean space), Schrödinger's Equation (which is a partial differential equation that describes how the quantum state of a physical system changes with time.), Unitary Operators, Quantum Circuits (in quantum information theory, a quantum circuit is a model for quantum computation in which a computation is a sequence of quantum gates, which are reversible transformations on a quantum mechanical analog of an n -bit register. This analogous structure is referred to as an n -qubit register.), Quantum Gates (in quantum computing and specifically the quantum circuit model of computation, a quantum gate or quantum logic gate is a basic quantum circuit operating on a small number of qubits), and Quantum Algorithms (in quantum computing, a quantum algorithm is an algorithm which runs on a realistic model of quantum computation, the most commonly used model being the quantum circuit model of computation) [1-4].

Nowadays, other concepts complement our knowledge about QuIn. The most important ones related to this work are:

Quantum Signal Processing (QSP) - The main idea is to take a classical signal, sample it, quantify it (for example, between 0 and 2^{-1}), use a classical-to-quantum interface, give an internal representation to that signal, process that quantum signal (denoising, compression, among others), measure the result, use a quantum-to-classical interface and subsequently detect the classical outcome signal. Interestingly, and as will be seen later, the quantum image processing has aroused more interest than QSP. In the words of its creator: "many new classes of signal processing algorithms have been developed by emulating the behavior of physical systems. There are also many examples in the signal processing literature in which new classes of algorithms have been developed by artificially imposing physical constraints on implementations that are not inherently subject to these constraints". Therefore, Quantum Signal Processing (QSP) is a signal processing framework [5, 6] that is aimed at developing new or modifying existing signal processing algorithms by borrowing from the principles of quantum mechanics and some of its interesting axioms and constraints. However, in contrast to such fields as quantum computing and quantum information theory, they do not inherently depend on the Physics associated with quantum mechanics. Consequently, in developing the QSP framework we are free to impose quantum mechanical constraints that we find useful and avoid those that are not. This framework provides a unifying conceptual structure for a variety of traditional processing techniques and a precise mathematical setting for developing generalizations and extensions of algorithms, leading to a potentially useful paradigm for signal processing with applications in areas including frame theory, quantization and sampling methods, detection, parameter estimation, covariance shaping, and multiuser wireless communication systems. The truth is that to date, there are few papers on this discipline and their practical use is close to null. Although they may introduce interesting ideas, they lack the purpose we need.

Quantum Image Processing (QImP) - is a young discipline which has been growing and developing, however, it is much more developed than QSP. QImP started in 1997. That year, Vlasov proposed a method of using quantum computation to recognize the so-called *orthogonal images* [7]. Five years later, in 2002, Schutzhold described a quantum algorithm that searches specific patterns in binary images [8]. A year later, in October 2003, Beach, Lomont, and Cohen from Cybernet Systems Corporation (an organization with a close cooperative relationship with the US Defense Department) demonstrated the possibility that quantum algorithms (such as Grover's algorithm) can be used in image processing. In that paper, they describe a method which uses a quantum algorithm to detect the posture of certain targets. Their study implies that quantum image processing may, in the future, play a valuable role during wartime [9].

Later, we can find the work of Venegas-Andraca [10], where he proposes quantum image representations such as Qubit Lattice [11, 12]; in fact, this is the first doctoral thesis in the specialty. History continues with the quantum image representation via the Real Ket [13] of Latorre Sentís, with a special interest in image compression in a quantum context. A new stage begins with the proposal of Le *et al.* [14], where Flexible

Representation of Quantum Images (FRQIs) provides a way to represent images on quantum computers in the form of a normalized state which captures information about colors and their corresponding positions in the images. History continues up to date by different authors and their innovative internal representation techniques of the image [15-36].

Very similar to the case of QSP, the idea behind QImP is to take a classic image (captured by a digital camera or photon counter) and place it in a quantum machine through a classical-to-quantum interface (this process is known as preparation of qubits). QImP gives some internal representation to the image using the procedures mentioned above and processing it (denoising and compressing, among others). Thus, obtaining the outcome via quantum measurement, which is the center of the quantum-to-classical interface. The contribution of a quantum machine over a classic machine, when it comes to processing images, is that the former has much more power of processing. This last advantage can handle images and algorithms of a high computational cost, which would be unmanageable in a classic machine in a practical sense, at least, this is the main idea for the future.

However, the problem of this discipline lies in its genetic, given that QuIP is the daughter of QuIn and DIP, thus, falling into the old dilemma of what to prioritize when teaching, i.e.: when teaching Latin to Peter, should we know more about Latin or more about Peter? The answer is simple: we should know both very well, however this is when the mission becomes impossible because a trade-off between DIP and QuIn exists. In other words, what is acceptable in QuIn is (at the same time) inadmissible in DIP. See more detail about this serious practical problem in [37].

The problem mentioned above begins with quantum measurement. If after quantum processing the quantum image within the quantum computer, we want to retrieve the result by tomography of quantum states, we will encounter a serious obstacle. In fact, if we make a tomography of quantum states in QIP (even, this can be extended to any method of quantum measurement after the tomography) with an error of 6% in our knowledge of the state, this constitutes an excellent measure of such state [38–41], but on the other hand, and this time from the standpoint of DIP [42-45], an error of 6% in each pixel of the outcome image constitutes a disaster, since this error becomes an unmanageable and exaggerated noise. So overwhelming is the aforementioned disaster that the recovered image loses its visual intelligibility, i.e., its look and feel, and morphology due to the destruction of edges and textures.

This clearly means (and for this purpose, one need only read the papers of QImP cited above) that these works are based on computer simulations in classical machines, exclusively (in most cases in MATLAB® [46]), and they do not represent test in a laboratory of Quantum Physics. In fact, if these field trials were held, the results would be the aforementioned. We only have to go to the lab and try with a single pixel of an image, then extrapolate the results to the entire image and the inconvenience will be explicit. On the other hand, today there are obvious difficulties to treat a full image inside a quantum machine, however, there is no difficulty for a single pixel, since that pixel represents a single qubit, and this can be tested in any laboratory in the world, without problems. Therefore, there are no excuses [37].

Definitely, the problem lies in the hostile relationship between the internal representation of the image (inside quantum machine), and the outcome measurement is the recovery of the image outside of quantum machine. Thus, the only technique of QImP that survives is Quantum Boolean Image Processing (QBImP) [47]. This is because it works with CBS, exclusively, and the quantum measurement does not affect the value of states. However, it is important to clarify that both, i.e., traditional techniques QImP and QBImP share a common enemy, and this is the decoherence [1, 47].

Quantum Fourier Transform (QFT) - In quantum computing, the QFT is a linear transformation on quantum bits and is the quantum analogue of the discrete Fourier transform. The QFT is a part of many quantum algorithms: notably Shor's algorithm for factoring and computing the discrete logarithm, the quantum phase estimation algorithm for estimating the eigenvalues of a unitary operator, and algorithms for the hidden subgroup problem.

The QFT can be performed efficiently on a quantum computer, with a particular decomposition into a product of simpler unitary matrices. Using a simple decomposition, the discrete Fourier transform can be implemented as a quantum circuit consisting of only $O(n^2)$ Hadamard gates and controlled phase shift gates, where n is the number of qubits [1]. This can be compared with the classical discrete Fourier transform, which takes $O(2n^2)$ gates (where n is the number of bits), which is exponentially more than $O(n^2)$. However, the quantum Fourier transform acts on a quantum state, whereas the classical Fourier transform acts on a vector, so not every task that uses the classical Fourier transform can take advantage of this exponential speedup. The best QFT algorithms known today require only $O(n \log n)$ gates to achieve an efficient approximation [48].

Finally, this work is organized as follows: Fourier Theory is outlined in Section 2, where we present the following concepts: continuous, discrete, and fast Fourier transform. In Section 3, we show the proposed new spectral methods with its consequences. Section 4 provides conclusions and a proposal for future works.

2 Fourier's Theory

In this section, we discuss the tools, which are key to understand the full extent to QSA. These tools are: Continuous, Discrete (DFT), and Fast Fourier Transform (FFT). These tools are developed until the main concept of *uncertainty principle*, which is fundamental to understand the theory behind QSA-FIT.

Other transformations (which are members of Fourier Theory too) like Fractional Fourier Transform (FRFT), Short-Time Fourier Transform (STFT), and Gabor transform (GT), make a poor contribution to solving the problems of the Fourier Theory described in the abstract (i.e., the need for a time-dependent spectrum analysis), including (without doubt) the wavelet transform in general and Haar basis in particular.

At the end of this section the ubiquity of QSA in the context of a much larger, modern and full spectral analysis should be clear. On the other hand, this section will allow us to better understand the role QSA as the origin of several tools used today in DSP, DIP, QSP and QImp. Finally, it will be clear why we say that QSA completes a set of tools which up to date are incomplete.

2.1 DFT and FFT

In this section, we discuss the main characteristics of classical versions of Fourier transforms [49-56], that is to say, continuous-time, discrete, fractional, short-time, and Gabor as well as the versions based on the cosine [51-56]. The quantum version is also included. Their strengths and weaknesses are covered in this section. However, none of them quite fill the gap in the field of spectral analysis. Finally, and in a strict relation to this paper, the unique practice difference between DFT and FFT is their computational cost.

2.1.1 Fourier transform

The Fourier transform decomposes a function of time (i.e., a *signal*) into the frequencies that makes it up, similarly to how a musical chord can be expressed as the amplitude (or loudness) of its constituent notes. The Fourier transform of a function of time itself is a complex-valued function of frequency, whose absolute value represents the amount of that frequency present in the original function, and whose complex argument is the phase offset of the basic sinusoid in that frequency. The Fourier transform is called the *frequency domain representation* (FDR) of the original signal. The term *Fourier transform* refers to both the FDR and the mathematical operation that associates the FRD to a function of time. The Fourier transform is not limited to functions of time, but in order to have a unified language, the domain of the original function is commonly referred to as the *time domain*. For many functions of practical interest one can define an operation that reverses this: the *inverse Fourier transformation* (also called *Fourier synthesis*) of a FRD which combines the contributions of all the different frequencies to recover the original function of time [49].

Linear operations performed in one domain (time or frequency) have corresponding operations in the other

domain, which are sometimes easier to perform. The operation of differentiation in the time domain corresponds to multiplication by the frequency so some differential equations are easier to analyze in the frequency domain. Also, convolution in the time domain corresponds to ordinary multiplication in the frequency domain. Concretely, this means that any linear time-invariant system, such as a filter applied to a signal, can be expressed relatively simply as an operation on frequencies. After performing the desired operations, transformation of the result can be made back to the time domain. Harmonic analysis is the systematic study of the relationship between the frequency and time domains, including the kinds of functions or operations that are "simpler" in one way or another, and has deep connections to almost all areas of modern mathematics [49].

Functions that are localized in the time domain have Fourier transforms that are spread out across the frequency domain and vice versa, a phenomenon known as the uncertainty principle. The critical case for this principle is the Gaussian function of substantial importance in probability theory and statistics as well as in the study of physical phenomena exhibiting normal distribution (e.g., diffusion). The Fourier transform of a Gaussian function is another Gaussian function. Joseph Fourier introduced the transform in his study of heat transfer, where Gaussian functions appear as solutions of the heat equation [49].

There are several common conventions (see, [49]) for defining the Fourier transform \hat{f} of an integrable function $f: \mathbb{R} \rightarrow \mathbb{C}$. In this paper, the following definition will be used:

$$\hat{f}(\xi) = \int_{-\infty}^{\infty} f(x) e^{-2\pi i x \xi} dx, \quad \text{for any real number } \xi. \quad (1)$$

When the independent variable x represents *time* (with SI unit of seconds), the transform variable ξ represents frequency (in hertz). Under suitable conditions f is determined by \hat{f} via the inverse transform:

$$f(x) = \int_{-\infty}^{\infty} \hat{f}(\xi) e^{2\pi i x \xi} d\xi, \quad \text{for any real number } x. \quad (2)$$

The statement that f can be reconstructed from \hat{f} is known as the Fourier inversion theorem, and was first introduced in Fourier's *Analytical Theory of Heat*, although what would be considered a proof by modern standards was not given until much later. The functions f and \hat{f} often are referred to as a *Fourier integral pair* or *Fourier transform pair* [49].

For other common conventions and notations, including the use of the angular frequency ω instead of the frequency ξ , see [49]. The Fourier transform on Euclidean space is treated separately, in which the variable x often represents position and ξ momentum.

Notes:

- In practice, the continuous-time version of the cosine transform is not used. Therefore, we will omit it in this work.
- The properties of the Fourier transform will be seen in the next subsection, that is, for Discrete Fourier Transform (DFT), although only the most relevant in terms of this work will be introduced.
- The two-dimensional version of the Fourier transform will be not described here. Instead, for any subsequent versions, the property known as separability [51-56] will be used.
- Any extension on the Fourier transform shown in [49, 50].

2.1.2 DFT

In mathematics, the discrete Fourier transform (DFT) converts a finite list of equally spaced samples of a function into the list of coefficients of a finite combination of complex sinusoids ordered by their frequencies that have those same sample values. It can be said to convert the sampled function from its original domain (often time or position along a line) to the frequency domain [51].

The input samples are complex numbers (in practice, they are usually real numbers) and the output coefficients are complex as well. The frequencies of the output sinusoids are integer multiples of a fundamental frequency, whose corresponding period is the length of the sampling interval. The combination of sinusoids obtained through the DFT is therefore periodic with that same period. The DFT differs from the discrete-time Fourier transform (DTFT) in that its input and output sequences are both finite; therefore, it is said to be the Fourier analysis of finite-domain-discrete-time functions (or periodic) [51].

Since it deals with a finite amount of data, it can be implemented in computers by numerical algorithms or even dedicated hardware. These implementations usually employ efficient fast Fourier transform (FFT) algorithms; so much so that the terms "FFT" and "DFT" are often used interchangeably. Prior to its current usage, the "FFT" initialism may have also been used for the ambiguous term "finite Fourier transform" [51].

The sequence of N complex numbers x_0, x_1, \dots, x_{N-1} is transformed into an N -periodic sequence of complex numbers:

$$X_k @ \sum_{n=0}^{N-1} x_n \cdot e^{-2\pi i k n / N}, \quad k \in \mathbf{Z} \text{ (integers)} \quad (3)$$

Each X_k is a complex number that encodes both amplitude and phase of a sinusoidal component of function x_n . The sinusoid's frequency is k cycles per N samples. Its amplitude and phase are:

$$|X_k|/N = \sqrt{\text{Re}(X_k)^2 + \text{Im}(X_k)^2} / N \quad (4)$$

$$\arg(X_k) = \text{atan2}(\text{Im}(X_k), \text{Re}(X_k)) = -i \ln \left(\frac{X_k}{|X_k|} \right),$$

where atan2 is the two-argument form of the arctan function. Assuming periodicity (see Periodicity in [51]), the customary domain of k computed is, actually, $[0, N-1]$. That is always the case when the DFT is implemented via the Fast Fourier transform algorithm. But other common domains are $[-N/2, N/2-1]$ (N even) and $[-(N-1)/2, (N-1)/2]$ (N odd) as when the left and right halves of an FFT output sequence are swapped. Finally, out of all its properties, the most important ones for this paper are the following [51-56]:

The unitary DFT - Another way of looking at the DFT is to note that in the above discussion, the DFT can be expressed as a Vandermonde matrix, introduced by Sylvester in 1867,

$$F = \begin{bmatrix} \omega_N^{00} & \omega_N^{01} & \text{L} & \omega_N^{0(N-1)} \\ \omega_N^{10} & \omega_N^{11} & \text{L} & \omega_N^{1(N-1)} \\ \text{M} & \text{M} & \text{O} & \text{M} \\ \omega_N^{(N-1)0} & \omega_N^{(N-1)1} & \text{L} & \omega_N^{(N-1)(N-1)} \end{bmatrix} \quad (5)$$

where

$$\omega_N = e^{-2\pi i / N} \quad (6)$$

is a primitive N th root of unity called twiddle factor.

While for the case of discrete cosine transform (DCT), we have:

$$\omega_N = \cos(2\pi/N) \quad (7)$$

The inverse transform is then given by the inverse of the above matrix,

$$F^{-1} = \frac{1}{N} F^* \quad (8)$$

For unitary normalization, we use a constant like $1/\sqrt{N}$, then, the DFT becomes a unitary transformation, defined by a unitary matrix:

$$\begin{aligned} U &= F/\sqrt{N} \\ U^{-1} &= U^* \\ |\det(U)| &= 1 \end{aligned} \quad (9)$$

where $\det(\bullet)$ is the *determinant function of* (\bullet) , and $(\bullet)^*$ means *conjugate transpose of* (\bullet) .

All this shows that the DFT is the product of a matrix by a vector, essentially, as follows:

$$\begin{bmatrix} X_0 \\ X_1 \\ \vdots \\ X_{N-1} \end{bmatrix} = \begin{bmatrix} \omega_N^{00} & \omega_N^{01} & \dots & \omega_N^{0(N-1)} \\ \omega_N^{10} & \omega_N^{11} & \dots & \omega_N^{1(N-1)} \\ \vdots & \vdots & \ddots & \vdots \\ \omega_N^{(N-1)0} & \omega_N^{(N-1)1} & \dots & \omega_N^{(N-1)(N-1)} \end{bmatrix} \begin{bmatrix} x_0 \\ x_1 \\ \vdots \\ x_{N-1} \end{bmatrix} \quad (10)$$

No Compact Support – Based on Eq.(10), we can see that each element X_k of output vector results from multiplying the k th row of the matrix by the complete input vector, that is to say, each element X_k of output vector contains every element of the input vector. A direct consequence of this is that DFT scatters the energy to its output, in other words, DFT has a disastrous treatment of the output energy. Therefore, no compact support is equivalent to:

- DFT has a bad treatment of energy at the output, and
- DFT is not a time-varying transform, but a frequency-varying transform.

Time-domain vs frequency-domain measurements – As we can see in Fig.1, thanks to DFT we have a new perspective regarding to signals measurement, i.e., the spectral viewing [55, 56].

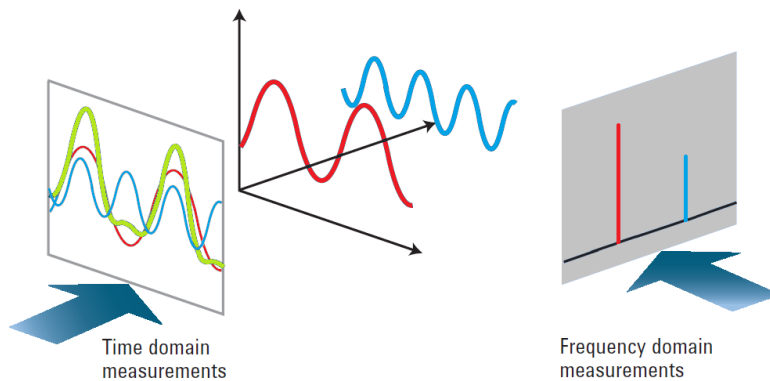


Fig. 1 Time domain vs frequency domain measurements.

Both point of view allow us to make a nearly complete analysis of the main characteristics of the signal [51-56]. As we can see in Eq.(10), DFT is the result product between a complex matrix by a real vector (signal). This gives us a vector output which is also complex [55, 56]. Therefore, for practical reasons, it is more useful to use the Power Spectral Density (PSD) [51-56].

On the other hand, if we rewrite Eq.(10), we will have

$$X = Fx \quad (11)$$

where X is the output vector (in frequency domain), F is the DFT matrix (see Eq.5), and x is the input vector (in time domain), then

$$\text{PSD} = \frac{X \times \text{conj}(X)}{NFFT \times L} \quad (12)$$

In Eq.(12), “ \times ” means infix version of Hadamard’s product of vectors [57], e.g., if we have two vectors $A = \{a_0, \dots, a_{N-1}\}$ and $B = \{b_0, \dots, b_{N-1}\}$, then $A \times B = \{a_0 b_0, a_1 b_1, \dots, a_{N-1} b_{N-1}\}$, while $\text{conj}(\bullet)$ means *complex conjugate of* (\bullet), and, “ \times ” means simply product of scalars.

In DSP, some authors work with the square root of PSD [51-54], and others - on the contrary - with the modulus (or absolute value) of X [55, 56], directly.

Spectral analysis - When the DFT is used for signal spectral analysis, the $\{x_n\}$ sequence usually represents a finite set of uniformly spaced time-samples of some signal $x(t)$, where t represents time. The conversion from continuous time to samples (i.e., discrete-time) changes the underlying Fourier transform of $x(t)$ into a discrete-time Fourier transform (DTFT), which generally entails a type of distortion called aliasing. The key to minimizing that distortion is to choose an appropriate sample-rate (see *Nyquist rate*). Similarly, the conversion from a very long (or infinite) sequence to a manageable size entails a type of distortion called *leakage*, which is manifested as a loss of detail (a.k.a. resolution) in the DTFT. The choice of an appropriate sub-sequence length is the primary key to minimizing that effect. When the available data (and time to process it) is more than the amount needed to attain the desired frequency resolution, a standard technique is to perform multiple DFTs, for example as when creating a spectrogram. If the desired result is a power spectrum and noise or randomness is present in the data, averaging the magnitude components of the multiple DFTs is a useful procedure to reduce the variance of the spectrum (also called a periodogram in this context). Two examples of such techniques are the Welch method and the Bartlett method; the general subject of estimating the power spectrum of a noisy signal is called spectral estimation.

A final source of distortion (or perhaps *illusion*) is the DFT itself, because it is just a discrete sampling of the DTFT, which is a function of a continuous frequency domain which can be mitigated by increasing the resolution of the DFT. That procedure is illustrated at sampling the DTFT [55, 56].

- The procedure is sometimes referred to as *zero-padding*, which is a particular implementation used in conjunction with the FFT algorithm. The inefficiency of performing multiplications and additions with zero-valued *samples* is more than offset by the inherent efficiency of the FFT.
- As already noted, leakage imposes a limit on the inherent resolution of the DTFT. So there is a practical limit to the benefit that can be obtained from a fine-grained DFT.

Summing-up, we mention the most important advantages and disadvantages of DFT.

Disadvantages of DFT:

- fails at the edges. This is the reason why in the JPEG algorithm (employed in image compression) DCT is used instead of DFT [42-45]. Even, discrete Hartley transform outperforms DFT in DSP and DIP [42, 43].

- does not have compact support. To arrive at the frequency domain the correspondence element by element between the two domains (time and frequency) is lost, with a lousy treatment of energy.
- loses the time correspondence as a consequence of not having compact support. In fact, it moves away from the time domain. For this reason, in the last decades, the scientific community has created some palliatives with better performance in both domains simultaneously, i.e., time and frequency, such tools are: STFT, GT, and wavelets.
- has phase uncertainties (i.e., indeterminate phase for magnitude = 0) [55, 56].
- has a big computational cost as it arises from the product of a matrix by a vector. Its computational cost is $O(N^2)$ for signals (1D), and $O(N^4)$ for images (2D).

All this would seem to indicate that it is a bad transform, however, it is its advantages that keep it afloat. Some of them will be described below.

Advantages:

- It is at its optimum state for filtering and compression, since the decisions are taken in the spectral domain. Although as we mentioned before, given its problem with the edges, we use DCT instead of DFT.
- It makes the convolutions easier when the fast release of DFT is used (i.e., FFT).
- It complies with the separability property, which is extremely useful when DFT should be applied to two and three-dimensional arrays [42-45].
- It allows faster versions of itself, such as FFT, due to its internal canonical form (distribution of twiddle factors within the DFT matrix).

2.1.3 FFT

Fast Fourier Transform - FFT inherits all the disadvantages of the DFT, except for its computational complexity. In fact, and unlike DFT, the computational cost of FFT is $O(N \cdot \log_2 N)$ for signals (1D), and $O((N \cdot \log_2 N)^2)$ for images (2D). For this reason, it is called fast Fourier transform.

FFT is an algorithm that computes the direct form of Discrete Fourier Transform (DFT) of a sequence, or its inverse. Fourier analysis converts a signal from its original domain (often time or space) to the frequency domain and vice versa. An FFT rapidly computes such transformations by factorizing the DFT matrix into a product of sparse (mostly zero) factors [58, 59]. As a result, it manages to reduce the complexity of computing the DFT from $O(N^2)$, which arises if one simply applies the definition of DFT, to $O(N \cdot \log_2 N)$, where N is the data size. The computational cost for this technique is never greater than the conventional approach and usually significantly less. Further, the computational cost as a function of n is highly continuous, so that linear convolutions of sizes are somewhat larger than a power of two.

FFT is widely used for many applications in engineering, science, and mathematics. The basic ideas underlying FFT were popularized in 1965, but some algorithms had been derived as early as 1805 [60]. In 1994 Gilbert Strang described the fast Fourier transform as *the most important numerical algorithm of our lifetime* [61] and it was included in the Top 10 Algorithms of 20th Century by the IEEE journal on Computing in Science & Engineering [62].

Overview - There are many different FFT algorithms involving a wide range of mathematics from a simple Arithmetic of complex-numbers to Group Theory and Number Theory. This article gives an overview of the available techniques and some of their general properties while the specific algorithms are described in subsidiary articles linked below.

The best known FFT algorithms depend upon the factorization of N , but there are FFTs with $O(N \cdot \log_2 N)$ complexity for all N , even for prime N . Many FFT algorithms only depend on the fact that $e^{-2\pi i/N}$ is an N -th primitive root of unity, and thus can be applied to analogous transforms over any finite field, such as number-theoretic transforms. Since the inverse DFT is the same as the DFT, but with the opposite sign in the exponent and a $1/N$ factor, any FFT algorithm can easily be adapted for it.

2.1.4 Other transforms

- The *short-time Fourier transform (STFT)*, or alternatively *short-term Fourier transform*, is a Fourier-related transform used to determine the sinusoidal frequency and phase content of local sections of a signal as it changes over time [63, 64]. In practice, the procedure for computing STFT is to divide a longer time signal into shorter segments of equal length and then compute the Fourier transform separately on each shorter segment. This reveals the Fourier spectrum on each shorter segment. Then, STFT is usually plotted by the changing spectra as a function of time [63-67].
- The *Gabor transform (GT)* is a special case of the short-time Fourier transform. It is used to determine the sinusoidal frequency and phase content of local sections of a signal as it changes over time [64, 67]. This simplification allows a practical and realizable Gabor transform with the possibility of using very important applications, such as: face and fingerprint recognition, textured features and classification, facial expression classification, face reconstruction, fingerprint recognition, facial landmark location, and iris recognition [42-45], among others.
- In mathematics, in the area of harmonic analysis, the *fractional Fourier transform (FRFT)* is a family of linear transformations generalizing the Fourier transform [68-81]. It can be thought of as the Fourier transform to the n -th power, where n does not need to be an integer - thus, it can transform a function to any *intermediate* domain between time and frequency. Its applications range from filter design and signal analysis to phase retrieval and pattern recognition.
- The *wavelet transform (WT)* is based on a *wavelet series*, which is a representation of a square-integrable (real-or complex-valued) function by a certain orthonormal series generated by a wavelet. Nowadays, WT is one of the most popular candidates of the time-frequency-transformations [82-131].

Nevertheless, these internal and external improvements to the Fourier Theory (respectively) do not represent a practical contribution in determining the spectral components (frequency) of a signal for each instant.

2.2 Fourier Uncertainty Principle

In quantum mechanics, the uncertainty principle [132], also known as Heisenberg's uncertainty principle (HUP), is any of a variety of mathematical inequalities asserting a fundamental limit to the precision with which certain pairs of physical properties of a particle can be known simultaneously. That is to say, since these physical properties are complementary variables, we cannot know energy E and time t , or, momentum p and position x , at the same time. In other words, they cannot be simultaneously measured with arbitrarily high precision, as there is a minimum value for the product of the uncertainties of these two measurements. HUP was introduced first in 1927 by the German physicist Werner Heisenberg, it states that the more precisely the position of some particle is determined, the less precisely its momentum can be known, and vice versa. The formal inequality regarding the uncertainty of energy ΔE and the uncertainty of time Δt was derived by Earle Hesse Kennard later that year and by Hermann Weyl in 1928:

$$\Delta E \Delta t \geq \hbar/2 \quad (13)$$

where \hbar is the reduced Planck constant, $h / 2\pi$. The energy associated to such system is

$$E = \hbar\omega \quad (14)$$

where $\omega = 2\pi f$, being f the frequency, and ω the angular frequency.

Then, any uncertainty about ω is transferred to the energy, that is to say,

$$\Delta E = \hbar\Delta\omega \quad (15)$$

Replacing Eq.(15) into (13), we will have,

$$h \Delta\omega \Delta t \geq h/2 \quad (16)$$

Finally, simplifying Eq.(16) will result in,

$$\Delta\omega \Delta t \geq 1/2. \quad (17)$$

Equation (17) says that a simultaneous decimation in time and frequency is impossible for FFT. Therefore, we must decimate in time or frequency, but not both at once. The last four transforms (STFT, GT, FrFT, and WT) represent a futile effort -to date- to link each sample in time with its counterpart in frequency thanks to a biunivocal correspondence in a more closely (individually) way. That is to say, they are transforms without compact support. Although one of them (WT) sometimes has compact support [82-131].

3 Quantum Spectral Analysis (QSA)

3.1 In the beginning ... Schrödinger's equation

3.1.1 Qubits and Bloch's sphere

The bit is the fundamental concept of classical computation and classical information. Quantum computation and quantum information are built upon an analogous concept, the quantum bit, or qubit for short. In this section we introduce the properties of single and multiple qubits, comparing and contrasting their properties to those of classical bits [1]. The difference between bits and qubits is that the latter can be in a state other than $|0\rangle$ or $|1\rangle$ [1, 2]. It is also possible to form linear combinations of states, often called superposition:

$$|\psi\rangle = \alpha|0\rangle + \beta|1\rangle, \quad (18)$$

where $|\psi\rangle$ is called *wave function*, $|\alpha|^2 + |\beta|^2 = 1$, with the states $|0\rangle$ and $|1\rangle$ are understood as different polarization states of light. Besides, a column vector $|\psi\rangle$ is called a *ket* vector $[\alpha \ \beta]^T$, where, $(\bullet)^T$ means transpose of (\bullet) , while a row vector $\langle\psi|$ is called a *bra* vector $[\alpha \ \beta]$. Although α and β are complex numbers, for many purposes not much is lost by thinking of them as real numbers. Particularly, the state of a qubit is a vector in a two-dimensional complex vector space. The special states $|0\rangle$ and $|1\rangle$ are known as Computational Basis States (CBS), and form an orthonormal basis for this vector space, being

$$|0\rangle = \begin{bmatrix} 1 \\ 0 \end{bmatrix} \quad \text{and} \quad |1\rangle = \begin{bmatrix} 0 \\ 1 \end{bmatrix}.$$

One useful picture in thinking about qubits is the following geometric representation, where if $|\alpha|^2 + |\beta|^2 = 1$, then, we may rewrite Eq.(18) as

$$|\psi\rangle = e^{i\gamma} \left(\cos \frac{\theta}{2} |0\rangle + e^{i\phi} \sin \frac{\theta}{2} |1\rangle \right) = e^{i\gamma} \left(\cos \frac{\theta}{2} |0\rangle + (\cos \phi + i \sin \phi) \sin \frac{\theta}{2} |1\rangle \right) \quad (19)$$

where $0 \leq \theta \leq \pi$, $0 \leq \phi < 2\pi$. We can ignore the factor $e^{i\gamma}$ of Eq.(19), because it has no observable effects [1], and for that reason we can effectively write

$$|\psi\rangle = \cos \frac{\theta}{2} |0\rangle + e^{i\phi} \sin \frac{\theta}{2} |1\rangle \quad (20)$$

The numbers θ and ϕ define a point on the unit three-dimensional sphere, as shown in Fig.2.

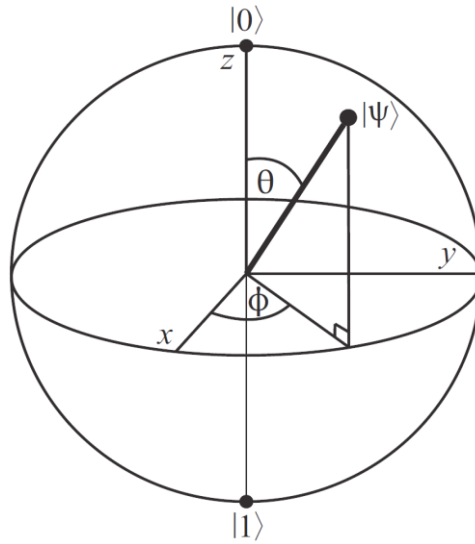


Fig. 2 Bloch's sphere.

Quantum mechanics is mathematically formulated in Hilbert space or projective Hilbert space. The space of pure states of a quantum system is given by the one-dimensional subspaces of the corresponding Hilbert space (or the "points" of the projective Hilbert space). In a two-dimensional Hilbert space, this is simply the complex projective line, which is a geometrical sphere often called the Bloch's sphere. In quantum information, it provides a useful means of visualizing the state of a single qubit, and often serves as an excellent testbed for ideas about quantum computation. Many of the operations on single qubits which can be seen in [1] are neatly described within the Bloch's sphere picture. However, it must be kept in mind that this intuition is limited because there is no simple generalization of the Bloch's sphere known for multiple qubits [1, 2]. Except in the case where $|\psi\rangle$ is one of the ket vectors $|0\rangle$ or $|1\rangle$ the representation is unique. The parameters θ and ϕ , re-interpreted as spherical coordinates, specify a point $\hat{a} = (\sin\theta \cos\phi, \sin\theta \sin\phi, \cos\theta)$ on the unit sphere in \mathbb{R}^3 according to Eq.(19).

Figure 3 highlights all components (details) concerning the Bloch's sphere, namely

$$\text{Spin down} = |\downarrow\rangle = |0\rangle = \begin{bmatrix} 1 \\ 0 \end{bmatrix} = \text{qubit basis state} = \text{North Pole} \quad (21)$$

and

$$\text{Spin up} = |\uparrow\rangle = |1\rangle = \begin{bmatrix} 0 \\ 1 \end{bmatrix} = \text{qubit basis state} = \text{South Pole} \quad (22)$$

Both poles play a fundamental role in the development of the quantum computing [1]. These poles represent a very important concept to the affections of the development quantum information processing, in particular, the notion of latitude (parallel) on the Bloch's sphere. Such parallel as shown in green in Fig.3, where we can see the complete coexistence of poles, parallels and meridians on the sphere, including computational basis states ($|0\rangle, |1\rangle$).

Finally, the poles and the parallels form the geometric bases of criteria and logic needed to implement any quantum gate or circuit.

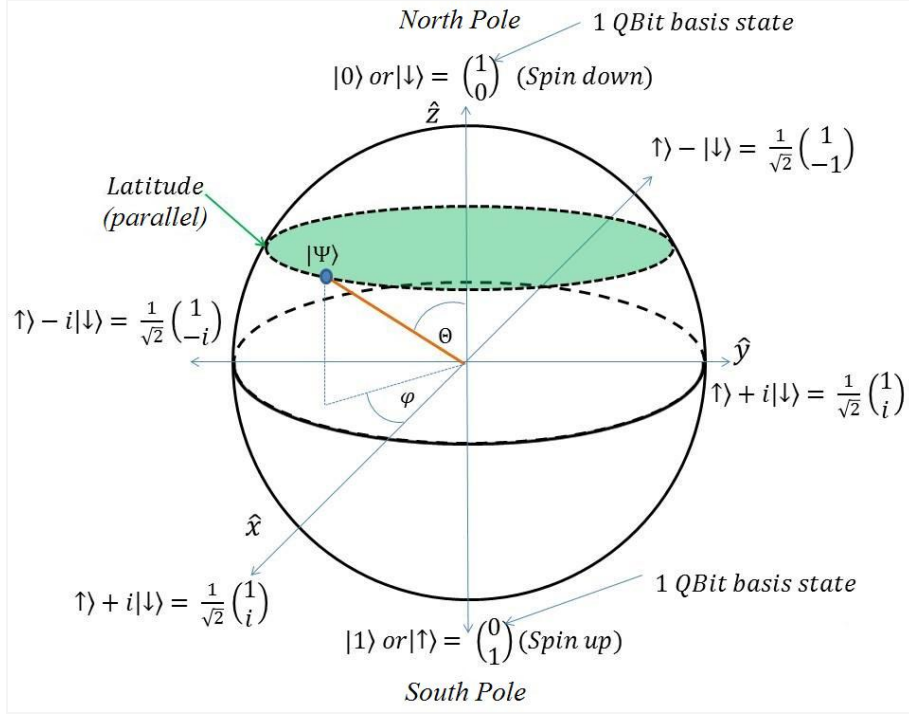


Fig. 3 Details of the poles, as well as an example of parallel and several qubit states on the sphere.

3.1.2 Schrödinger's equation and unitary operators

A quantum state can be transformed into another state thanks to a unitary operator, symbolized as U , i.e., $U : H \rightarrow H$ on a Hilbert space H , being called a unitary operator if it satisfies $U^\dagger U = U U^\dagger = I$, where $(\bullet)^\dagger$ is the adjoint of (\bullet) , and I is the identity matrix. U is required to preserve inner products: If we transform $|\chi\rangle$ and $|\psi\rangle$ to $U|\chi\rangle$ and $U|\psi\rangle$, then $\langle\chi|U^\dagger U|\psi\rangle = \langle\chi|\psi\rangle$. In particular, unitary operators preserve lengths:

$$\langle\psi|U^\dagger U|\psi\rangle = \langle\psi|\psi\rangle = 1, \text{ if } |\psi\rangle \text{ is on the Bloch's sphere (i.e., it is a pure state).} \quad (23)$$

On the other hand, the unitary operator satisfies the following differential equation known as the Schrödinger equation [1-4]:

$$\frac{d}{dt} U(t + \Delta t, t) = \frac{-i\hat{H}}{\hbar} U(t + \Delta t, t) \quad (24)$$

where \hat{H} represents the Hamiltonian matrix of the Schrödinger equation, $i = \sqrt{-1}$, and \hbar is the reduced Planck constant, i.e., $\hbar = h/2\pi$. Multiplying both sides of Eq.(24) by $|\psi(t)\rangle$ and setting

$$|\psi(t + \Delta t)\rangle = U(t + \Delta t, t)|\psi(t)\rangle, \quad (25)$$

being $U(t + \Delta t, t) = U(t + \Delta t - t) = U(\Delta t)$ a unitary transform (operator and matrix), yields

$$\frac{d}{dt} |\psi(t)\rangle = \frac{-i\hat{H}}{\hbar} |\psi(t)\rangle. \quad (26)$$

The solution to the Schrödinger equation is given by the Hamiltonian's exponential matrix, that is to say, the unitary operator:

$$U(t + \Delta t, t) = e^{\frac{-i\hat{H}\Delta t}{\hbar}} \quad (\text{if Hamiltonian is not time dependent}) \quad (27)$$

and

$$U(t + \Delta t, t) = e^{\frac{-i}{\hbar} \int_0^t \hat{H} dt} \quad (\text{if Hamiltonian is time dependent}) \quad (28)$$

Thus the probability amplitudes evolve across time according to the following equation:

$$|\psi(t + \Delta t)\rangle = e^{\frac{-i\hat{H}\Delta t}{\hbar}} |\psi(t)\rangle \quad (\text{if Hamiltonian is not time dependent}), \quad (29)$$

or

$$|\psi(t + \Delta t)\rangle = e^{\frac{-i}{\hbar} \int_0^t \hat{H} dt} |\psi(t)\rangle \quad (\text{if Hamiltonian is time dependent}). \quad (30)$$

Equation (29) is the main piece in building circuits, gates and quantum algorithms, being U who represents such elements [1].

Finally, the discrete version of Eq.(26) is

$$|\psi_{k+1}\rangle = \frac{-i\hat{H}}{\hbar} |\psi_k\rangle, \quad (31)$$

for a time dependent (or not) Hamiltonian, being k the discrete time.

3.1.3 Quantum Circuits, Gates, and Algorithms; Reversibility and Quantum Measurement

As we can see in Fig.4, and remember Eq.(25), the quantum algorithm (identical case to circuits and gates) viewed as a transfer (or mapping input-to-output) has two types of outputs:

- a) the result of algorithm (circuit of gate), i.e., $|\psi_n\rangle$, with $n = \Delta k$ and $k = 0$, or
- b) part of the input $|\psi_0\rangle$, i.e., $|\underline{\psi}_0\rangle$ (underlined $|\psi_0\rangle$), in order to impart reversibility to the circuit, which is a critical need in quantum computing [1].

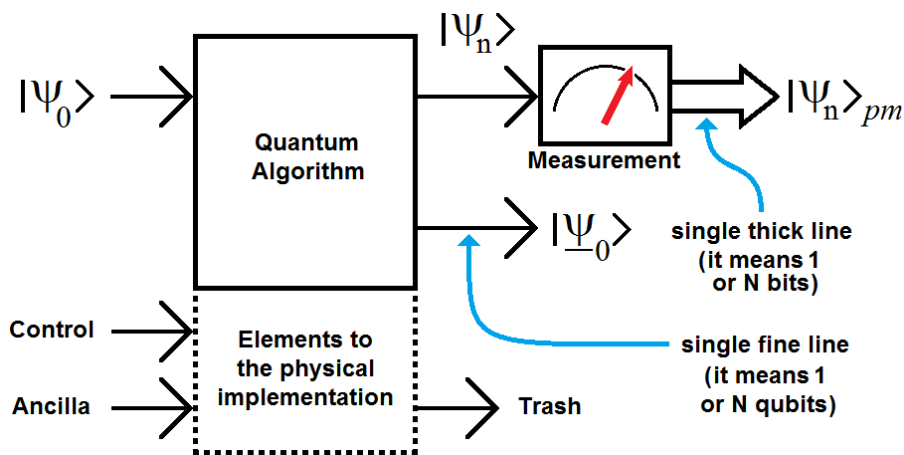


Fig. 4 Module to measuring, quantum algorithm and the elements needs to its physical implementation.

Besides, the illustration clearly shows a module for measuring $|\psi_n\rangle$ with their respective output, i.e., $|\psi_n\rangle_{pm}$ (or, $|\psi_n\rangle$ post-measurement), and a number of elements needed for the physical implementation of the quantum algorithm (circuit or gate), namely: control, ancilla and trash [1].

In Fig.4 as well as in the rest of them (unlike [1]) a single fine line represents a wire carrying 1 qubit or N qubits (qudit), interchangeably, while a single thick line represents a wire carrying 1 or N classical bits, also interchangeably. However, the mentioned concept of reversibility is closely related to energy consumption, and hence to the Landauer's Principle [1].

On the other hand, computational complexity studies the amount of time and space required to solve a computational problem. Another important computational resource is energy. In [1], the authors show the energy requirements for computation. Surprisingly, it turns out that computation, both classical and quantum, can in principle be done without expending any energy. Energy consumption in computation is deeply linked to the reversibility of the computation. In other words, the need of the presence of $|\psi_0\rangle$ to the output of quantum gate [1] is inexcusable. However, in quantum mechanics, measurement is a non-trivial and highly counter-intuitive process. Firstly, because measurement outcomes are inherently probabilistic, i.e. regardless of the carefulness in the preparation of a measurement procedure, the possible outcomes of such measurement will be distributed according to a certain probability distribution. Secondly, once the measurement has been performed, a quantum system is unavoidably altered due to the interaction with the measurement apparatus. Consequently, for an arbitrary quantum system, pre-measurement and post-measurement quantum states are different in general [1].

Postulate. Quantum measurements are described by a set of measurement operators $\{\hat{M}_m\}$, index m labels the different measurement outcomes, which act on the state space of the system being measured. Measurement outcomes correspond to values of *observables*, such as position, energy and momentum, which are Hermitian operators [1] corresponding to physically measurable quantities.

Let $|\psi\rangle$ be the state of the quantum system immediately before the measurement. Then, the probability that results in m is

$$p(m) = \langle \psi | \hat{M}_m^\dagger \hat{M}_m | \psi \rangle, \quad (32)$$

and the post-measurement quantum state is

$$|\psi\rangle_{pm} = \frac{\hat{M}_m |\psi\rangle}{\sqrt{\langle \psi | \hat{M}_m^\dagger \hat{M}_m | \psi \rangle}}. \quad (33)$$

Operators \hat{M}_m must satisfy the completeness relation of Eq.(34), because that guarantees that probabilities will sum to one; see Eq.(35) [1]:

$$\sum_m \hat{M}_m^\dagger \hat{M}_m = I \quad (34)$$

$$\sum_m \langle \psi | \hat{M}_m^\dagger \hat{M}_m | \psi \rangle = \sum_m p(m) = 1 \quad (35)$$

Let us work out a simple example. Assume we have a polarized photon with associated polarization orientations 'horizontal' and 'vertical'. The horizontal polarization direction is denoted by $|0\rangle$ and the vertical one by $|1\rangle$. Thus, an arbitrary initial state for our photon can be described by the quantum state $|\psi\rangle = \alpha|0\rangle + \beta|1\rangle$ (remembering Subsection 3.1.1, Eq.18), where α and β are complex numbers constrained

by the normalization condition $|\alpha|^2 + |\beta|^2 = 1$, and $\{|0\rangle, |1\rangle\}$ is the computational basis spanning H^2 . Then, we construct two measurement operators $\hat{M}_0 = |0\rangle\langle 0|$ and $\hat{M}_1 = |1\rangle\langle 1|$ and two measurement outcomes a_0, a_1 . After that, the full observable used for measurement in this experiment is $\hat{M} = a_0 |0\rangle\langle 0| + a_1 |1\rangle\langle 1|$. According to Postulate, the probabilities of obtaining outcome a_0 or outcome a_1 are given by $p(a_0) = |\alpha|^2$ and $p(a_1) = |\beta|^2$. Corresponding post-measurement quantum states are as follows: if outcome = a_0 , then $|\psi\rangle_{pm} = |0\rangle$; if outcome = a_1 then $|\psi\rangle_{pm} = |1\rangle$.

3.2 QSA properly speaking

Equation (26) represents the Schrödinger equation which will be simplified for better comprehension purposes

$$|\dot{\psi}(t)\rangle = -i \Omega(t) |\psi(t)\rangle, \quad (36)$$

where $|\dot{\psi}(t)\rangle = \frac{d}{dt} |\psi(t)\rangle$ and $\Omega(t) = \frac{\hat{H}(t)}{\hbar}$, being Ω the angular frequency matrix, and \hat{H} the Hamiltonian matrix. Both are simultaneously time dependents, i.e., we will have a matrix at each instant.

On the other hand, Ω depends on the respective –non relativistic– system, that is to say, where the most general form for one qubit is

$$\Omega(t) = \begin{bmatrix} \omega_{11}(t) & \omega_{12}(t) \\ \omega_{21}(t) & \omega_{22}(t) \end{bmatrix}. \quad (37)$$

Two interesting particular cases are represented by

$$\Omega(t) = \begin{bmatrix} \omega_1(t) & 0 \\ 0 & \omega_2(t) \end{bmatrix}, \quad (38)$$

and

$$\Omega(t) = \begin{bmatrix} \omega(t) & 0 \\ 0 & \omega(t) \end{bmatrix} = \omega(t) \begin{bmatrix} 1 & 0 \\ 0 & 1 \end{bmatrix} = \omega(t) I = \omega(t), \quad (39)$$

being I the identity matrix. Thus, replacing Eq.(39) into Eq.(36), the following will be obtained,

$$|\dot{\psi}(t)\rangle = -i \omega(t) |\psi(t)\rangle. \quad (40)$$

Next, we multiply both sides (by left) of Eq.(40) by $\langle \psi(t) |$,

$$\langle \psi(t) | \dot{\psi}(t) \rangle = -i \omega(t) \langle \psi(t) | \psi(t) \rangle. \quad (41)$$

Finally, $\omega(t)$ results in,

$$\omega(t) = i \frac{\langle \psi(t) | \dot{\psi}(t) \rangle}{\langle \psi(t) | \psi(t) \rangle}. \quad (42)$$

Equation (42) represents QSA for the monotone case. Now, we are going to multiply both sides (by right) of

Eq.(36) by $\langle \psi(t) |$, where Ω of Eq.(37) represents an irreducible matrix, therefore,

$$|\psi(t)\rangle\langle\psi(t)| = -i \Omega(t) |\psi(t)\rangle\langle\psi(t)| \quad (43)$$

Finally, $\Omega(t)$ results in,

$$\begin{aligned} \Omega(t) &= i |\psi(t)\rangle\langle\psi(t)| \left[|\psi(t)\rangle\langle\psi(t)| \right]^{-1} \\ &= i |\psi(t)\rangle\langle\psi(t)|^\dagger \end{aligned} \quad (44)$$

where

$$\langle\psi(t)|^\dagger = \langle\psi(t)| \left[|\psi(t)\rangle\langle\psi(t)| \right]^{-1} \quad (\text{is the pseudoinverse of } |\psi(t)\rangle) \quad (45)$$

Equation (44) represents QSA for the multitone case, however, in practice it is not used.

3.3 Frequency in time (FIT)

Once we have arrived to the classical world (after the collapse of the wave function), we can then apply an adaptation of QSA to classical signals called *frequency in time* (FIT). In fact, the experimental evidence indicates that FIT gives us the frequency of that classical signal at each time. Curiously, this concept is extensive to quantum signals too, including the case of classical and quantum images.

3.3.1 FIT for signals

In the classical version of Eq.(42) we are going to replace qubits by samples of a real signal, therefore, inner products disappear, and the classical version of Eq.(42) in a symbolic form is

$$\Delta\omega(t) = i \frac{1}{S(t)} \frac{\partial S(t)}{\partial t} = i \frac{\mathcal{S}(t)}{S(t)}, \quad (46)$$

where $\mathcal{S}(t) = \frac{\partial S(t)}{\partial t}$, and S is a signal defined in i^N , being N the size of the signal, and $\Delta\omega$ the frequency (before -in the context of Schrödinger equation- it is the imaginary angular frequency). Moreover, in certain cases Eq.(46) will be,

$$\Delta\omega(t) = i \frac{1}{S(t)} \frac{\Delta S(t)}{\Delta t} = i \frac{\mathcal{S}(t)}{S(t)}, \quad (47)$$

This happens because for gate (square signal with a flank with infinite slope in the transition) and semi-gate (square signal with a flank with finite slope in the transition) Eq.(46) and (47) give identical results. On the other hand, and appealing (for simplicity) to the discrete version of $\Delta\omega$, we will have,

$$\Delta\omega = i \mathcal{S}/S, \quad (48)$$

where “./” represents the infix version of Hadamard’s quotient of vectors [57], $S = [s_0 \ s_1 \ s_2 \ \dots \ s_{N-1}]$ is a signal of N samples, $\mathcal{S} = [\mathcal{S}_0 \ \mathcal{S}_1 \ \mathcal{S}_2 \ \dots \ \mathcal{S}_{N-1}]$ is its derivative, and $\Delta\omega = [\Delta\omega_0 \ \Delta\omega_1 \ \Delta\omega_2 \ \dots \ \Delta\omega_{N-1}]$ is the FIT of N samples. That is to say, for each sample, $\Delta\omega_n$ will be,

$$\Delta\omega_n = i \mathcal{S}_n / s_n \quad \forall n \in [0, N-1], \text{ being: } \mathcal{S}_n = (s_{n+1} - s_{n-1}) / 2, \text{ and } n \text{ the discrete time.} \quad (49)$$

Equation (49) is the discrete version of $\Delta\omega$ in its most inapplicable form, given that this is not applicable in cases where the denominator is zero (although unlike the FFT, $\Delta\omega$ has a definite value in FIT via a simple correction). Moreover, $\Delta\omega$ is an imaginary operator to be applied to real signals. Therefore, this form is called raw version. To overcome this drawback, we use an enhanced version based on *root mean square* (RMS) of the signal, as the following,

$$\Delta\omega_{RMS} = i \mathcal{F} / s_{RMS}, \quad (50)$$

where s_{RMS} –in its discrete form- is defined as follows [133]:

$$s_{RMS} = \sqrt{\frac{1}{N} \sum_{n=0}^{N-1} s_n^2}, \quad (51)$$

with,

$$\Delta\omega_{n,RMS} = i \mathcal{F}_n / s_{RMS}, \quad (52)$$

$\forall n \in [0, N-1]$. On the other hand, and to save the fact that $\Delta\omega$ is an imaginary operator to be applied to real signals, we will use (based on Eq.48) a more pure and useful version of *frequency in time* (FIT), i.e.:

$$\begin{aligned} \Delta\omega &= \sqrt{\Delta\omega \cdot \text{conj}(\Delta\omega)} \\ &= \sqrt{(i \mathcal{F} / S) \cdot \text{conj}(i \mathcal{F} / S)} \\ &= |\mathcal{F} / S| = |\mathcal{F}| / |S| = \frac{1}{|S|} \frac{|\Delta S|}{\Delta t} \end{aligned} \quad (53)$$

Being $\Delta f = \Delta\omega / 2\pi = [\Delta f_0 \ \Delta f_1 \ \Delta f_2 \ \dots \ \Delta f_{N-1}]$, the frequencies will be in hertz. Besides, $\Delta\omega$ is now a real operator to be applied to real signals. Remember that, this version (the original) depends on a possible denominator equal to zero, therefore, the next version directly dependent on the frequency based on Eq.(50) will be used:

$$\begin{aligned} \Delta f_{RMS} &= \frac{1}{2\pi} \sqrt{\Delta\omega_{RMS} \cdot \text{conj}(\Delta\omega_{RMS})} \\ &= \frac{1}{2\pi} \sqrt{(i \mathcal{F} / s_{RMS}) \cdot \text{conj}(i \mathcal{F} / s_{RMS})}, \\ &= \frac{1}{2\pi} |\mathcal{F} / s_{RMS}| \end{aligned} \quad (54)$$

that is to say,

$$\Delta f_{n,RMS} = \frac{1}{2\pi} |\mathcal{F}_n| / s_{RMS}, \quad \forall n \in [0, N-1] \quad (55)$$

Note: if $s_{RMS} = 0$, it means that the complete signal S is null in all its samples (i.e., $s_n = 0, \forall n \in [0, N-1]$) then $\Delta\omega_{n,RMS} = 0$, and hence, $\Delta f_{n,RMS} = 0, \forall n \in [0, N-1]$. In that case, we don't need spectral analysis.

Example - Next, we will implement the RMS version of FIT to a signal as shown in Fig.5, which is an electrocardiographic (ECG) signal of 80 pulses per second, with 256 samples per cycle. Top of Fig.5 shows the ECG, while its bottom shows the waterfall of ECG signal, where the positive peaks are clear, the negative peaks dark, and the intermediates gray.

On the other hand, Fig.6 shows the same signal of Fig.5: ECG of 80 cycles per second with 256 samples per cycle. However, in this case, ECG signal will be in blue, and FIT in red with their respective scales: ECG scale in blue to the left and FIT scale in red to the right. It is important to mention that the bottom of the figure shows a sequence of witness bars [134]. The distribution of such witness bars is in each case the FIT itself, where the accumulation of such bars has to do with the flanks of the original signal. In other words, the most pronounced flanks accumulate more bars, while less steep flanks accumulate fewer bars [134]. This means that the bars are witnessing an indirect flank detection, and based on FIT, the existing spectral components of the signal will have a steep flank [134].

As we can see in Fig.6, FIT is a flank detector that reacts with the spectral components which are represented by the degree of inclination of such flanks in time. Finally, in Fig.6, we can notice that FIT reaches the maximum where the signal has more pronounced flanks.

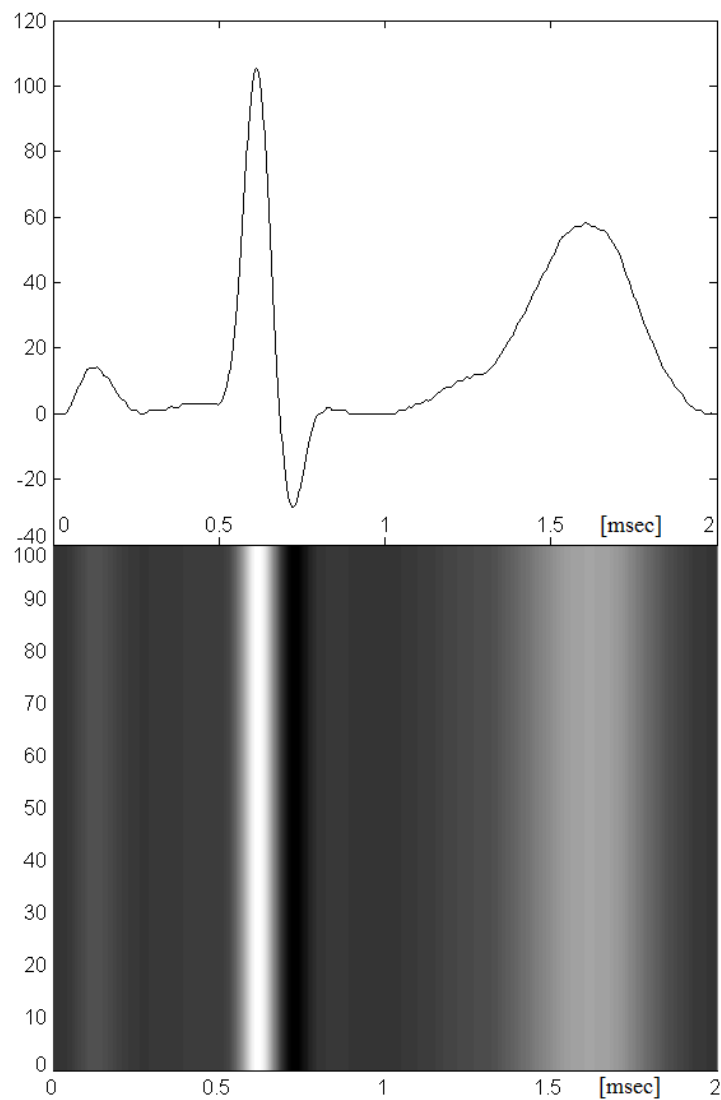


Fig. 5 Top: electrocardiographic signal. Bottom: its waterfall.

Finally, in [134] we can find several complementary versions of FIT for signals and images. Such versions imply the overlapping of samples (for signals) or pixels (for images) which are part of a mask (of the convolution type). In fact, this feature was used in both examples of this paper. However, it is important to clarify the existence of other versions based on no-overlapping masks, which generate approximation sub-bands (low frequency) and detail (high frequency), being very useful in many other applications [134].

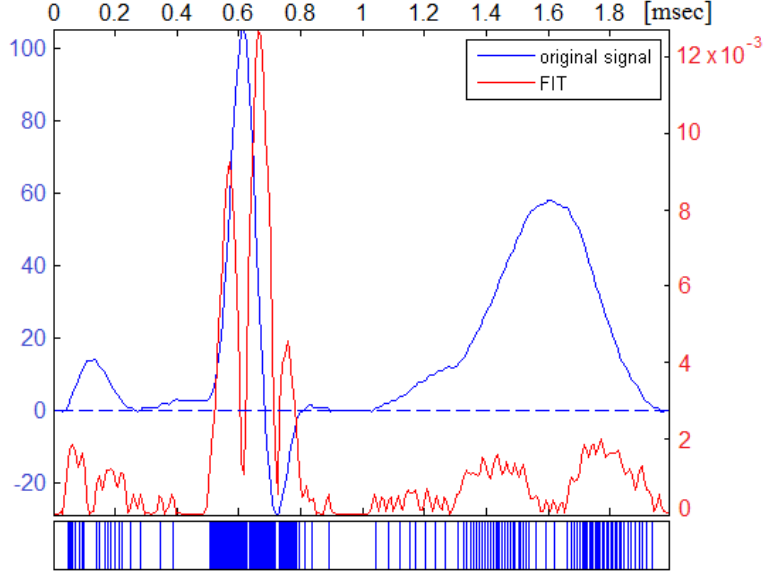


Fig. 6 Here, we have an ECG signal of 80 cycles per second with 256 samples in blue, while FIT is in red and a sequence of witness bars in blue at the bottom of the figure. The distribution of such witness bars is in a perfect relationship with the flank of the ECG signal, since the more pronounced flanks accumulate more bars, and the less steep flanks accumulate fewer bars in a perfect harmony with the peaks of FIT.

3.3.2 FIT for images

In the classical version of Eq.(42) but in the 2D case, and for each color channel (red-green-blue), we are going to replace qubits by pixels of a real image, therefore, for this case, FIT is represented by two directional components which depend on the direction of each derivative for each color.

Consequently, the image is padded depending on the size of the mask ($M = 3$, i.e., 3-by-3 pixels). If the image (e.g., for the case of the red channel: I_R) has a ROW-by-COL size, then, the padded I_R , or $I_{R,P}$ will have a $(ROW+2L)$ -by- $(COL+2L)$ size where $L = (M-1)/2$. Therefore, the original image I_R will be in the middle of the padded image $I_{R,P}$, which will have four lateral margins of L size to each side of I_R composed exclusively by zeros. Besides, we will have two masks, namely:

$$N_H = \frac{[-1 \ 0 \ 1]}{2}, \quad (\text{horizontal mask}), \text{ and} \quad (56)$$

$$N_V = N_H^T, \quad (\text{vertical mask}). \quad (57)$$

The procedure begins with a two-dimensional convolution between N_H and $I_{R,P}$ through a horizontal mask for vertical rafters:

$$I_H = N_H * I_{R,P} \quad (58)$$

After that, we continue with another two-dimensional convolution between N_V and $I_{R,P}$ through a vertical mask for horizontal rafters:

$$I_V = N_V * I_{R,P} \quad (59)$$

Finally, \mathcal{F} is obtained via Pythagoras between I_H and I_V ,

$$\mathcal{F} = \sqrt{I_H^2 + I_V^2} \quad (60)$$

Then, we obtain the two-dimensional version of Eq.(47):

$$\Delta\omega = i \mathcal{F}/I, \quad (61)$$

While, for each pixel, we will have,

$$\Delta\omega_{r,c} = i \mathcal{F}_{r,c} / I_{r,c} \quad \forall r \in [1, ROW], \text{ and } c \in [1, COL] \quad (62)$$

Similar to the signal case, Eq.(62) is the discrete version of $\Delta\omega$ in its most inapplicable form, given that this is not applicable in cases where the denominator is zero (although unlike the FFT, $\Delta\omega$ has a definite value in FIT via a simple correction). Moreover, $\Delta\omega$ is an imaginary operator to be applied to real images. Therefore, this form is called raw version. To overcome this drawback, we use an enhanced version based on *root mean square* (RMS) of the image, as the following one,

$$\Delta\omega_{eq} = i \mathcal{F}_{eq} / I_{eq}, \quad (63)$$

where the subscript “*eq*” means *equalized*. In general, the recommendation is to go from $[0, 2^8-1]$ to $[1, 2^8]$ for each pixel of each color channel for the image I .

In order to avoid the fact that $\Delta\omega$ is an imaginary operator applied to real images, a more pure and useful version of *frequency in time* (FIT) will be used (based on Eq.61):

$$\begin{aligned} \Delta\omega &= \sqrt{\Delta\omega \cdot \text{conj}(\Delta\omega)} \\ &= \sqrt{(i \mathcal{F}/I) \cdot \text{conj}(i \mathcal{F}/I)} \\ &= |\mathcal{F}/I| = |\mathcal{F}|/I \end{aligned} \quad (64)$$

The matrix $\Delta f = \Delta\omega / 2\pi$ has a size of ROW-by-COL with frequencies in hertz. Besides, $|I| = I$ since all values of each color channel are positive. It is important to remember that this version (raw) depends on a possible denominator equal to zero, therefore, based on Eq.(63) a new version directly dependent on the frequency will be applied:

$$\begin{aligned} \Delta f_{eq} &= \frac{1}{2\pi} \sqrt{\Delta\omega_{eq} \cdot \text{conj}(\Delta\omega_{eq})} \\ &= \frac{1}{2\pi} \sqrt{(i \mathcal{F}_{eq} / I_{eq}) \cdot \text{conj}(i \mathcal{F}_{eq} / I_{eq})} \\ &= \frac{1}{2\pi} |\mathcal{F}_{eq} / I_{eq}| = \frac{1}{2\pi} |\mathcal{F}_{eq}| / I_{eq} \end{aligned} \quad (65)$$

Note: here too, $|I_{eq}| = I_{eq}$, since all values of each color channel are positive.

Example - Next, the aforementioned version will be implemented selecting a color image: Angelina which is a picture of 1920-by-1080 pixels with 24 bit-per-pixel. See Fig.7.

Figure 8 shows the FIT operator over Angelina for the equalized version, where first-column-first-row is the original image, second-column-first-row is the red channel, first-column-second-row is the green channel, and second-column-second-row is the blue channel. Besides, in this figure, the texture and edges of the different color channels can be seen thanks to FIT. The same set of images shows Regions of Interest (ROIs) which include ergodic areas with a notable impact in the filtering (denoising) and compression contexts. Also, the FIT indicates the weight of each color over the main morphological characteristics of the image.



Fig. 7 Angelina: 1920-by-1080 pixels with 24 bpp.

Another important aspect to mention is that although Fig.7 and 8 have different scales, the amount of pixels (FIL-by-COL) is the same. Besides, we have manipulated the brightness and contrast for better display scroll of the three color channels.

Finally, FIT allows us to observe spectral components per pixel by color with a particular emphasis in texture and edges, which are notably important in applications such as visual intelligence for computer vision, image compression [134], filtering (denoising) [134], superresolution [134], forensic analysis of images, image restoration and enhancement [42-45].

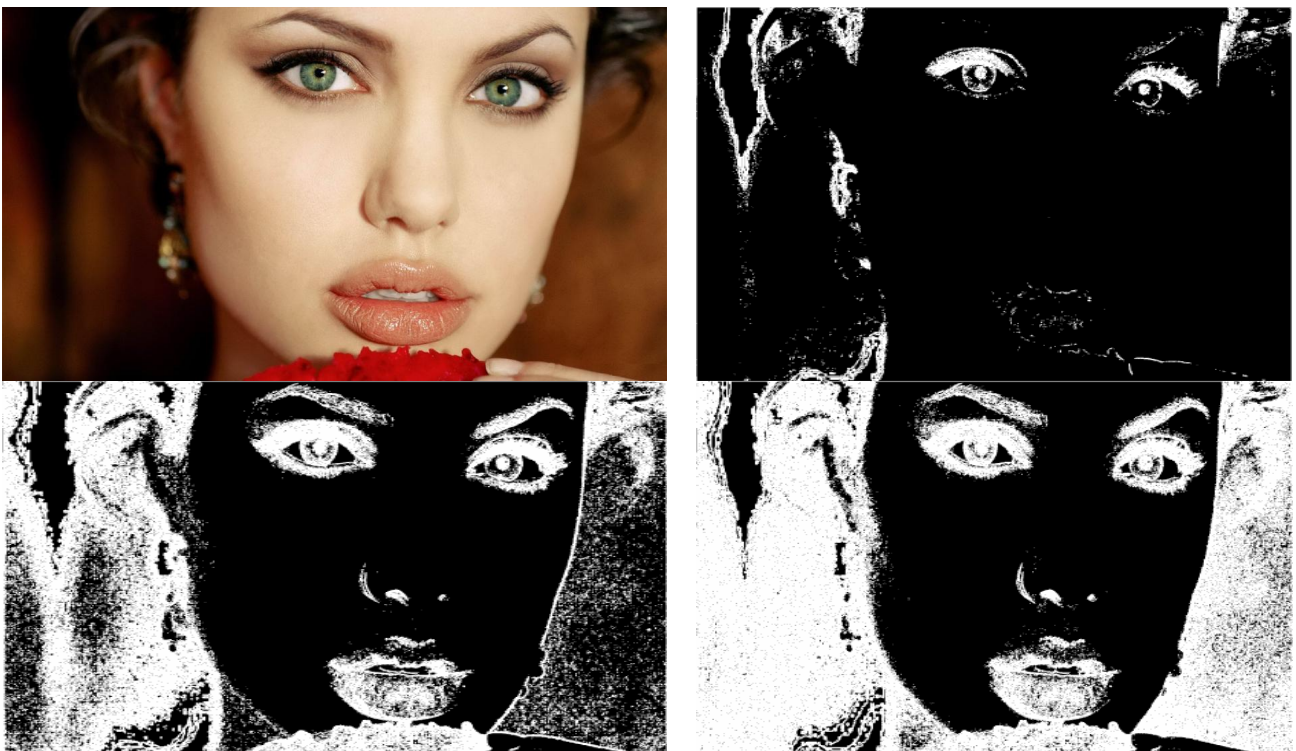


Fig.8 FIT operator is applied over Angelina for the equalized version, where first-column-first-row is the original image, second-column-first-row is the red channel, first-column-second-row is the green channel, and second-column-second-row is the blue channel.

As seen in the above example of FIT for signals, the effect of indeterminate FIT can be solved by the RMS version when a sample has a value equal to 0. However, the effect of indeterminate angle (phase) in FFT has no solution [135-138] when a sample has a value equal to 0. Besides, while FFT has no compact support, FIT has it. Compact support brings different treatment of energy to the output depending on the procedure, a lousy one by FFT and an excellent one by FIT. Another important comparative aspect between FFT and FIT is the poor performance of the FFT at the edges (both signals and images), whereby the FFT is replaced by the Fast Cosine Transform (FCT) in applications of compression and filtering [42-45]. This problem does not exist in FIT. Furthermore, FIT acts as a detector [134] which indicates that the encoding for the case of compression by the witness bar is similar to Position-Pulse-Modulation (PPM) or nonlinear sampling [139]. This means that it is very convenient to use the witness bars for both rows and columns on pictures as a new type of profilometry method instead of histograms [42-45], or as a complement of these [134]. Moreover, the advantages of nonlinear sampling are obvious in the reduction of consumed frequency in communications and signal compression [139].

Other relevant advantages of using FIT over FFT are as follow:

- FIT gives an instant notion of the spectral components of the signal or image. In other words, FIT demonstrates direct responsibility of flanks on the characteristics and values of such spectral components.
- FIT is responsive to ergodicity, the *regions of interest* (ROIs), textures, noises, flanks or edges tilt and their relationship with Shannon and Nyquist in nonlinear sampling for communications [139].
- FFT loses the link with time because it doesn't have compact support [134].
- FIT can be easily calibrated and related with FFT. See Figures (9) and (10).
- FIT gives frequency in terms of time directly: $\Delta f(t) = \Delta \omega(t) / (2\pi)$.
- Two-dimensional QSA-FIT is directional, and via Pythagoras it is consistent with the idea of directional QSA for images and N-dimensional arrays.
- In the case of FIT, the convolution mask is, in itself, a direct filtering process (denoising). It can be seen in detail in [134].
- In FIT, everything is parallelizable, therefore, the use of General-purpose graphics processing units (GPGPUs) is recommended [140], being FIT faster than FFT on them.
- In FIT, the Hamiltonian's basal tone [1] is associated with the spectral bands directly, making calibration considerably easier. Consequently, it turns out to be as simple as tuning an instrument. In fact, FIT is the chosen spectral analyzer when the resources are limited.
- Flank detection is equivalent to edge detection in visual intelligence. Besides, FIT detects the sign change and texture, and thus, assesses how an image is compressed. From the point of view of Information Theory [1], FIT also allows a nonlinear sampling which is more efficient than the traditional linear sampling currently being employed. In fact, QSA-FIT can perform edge detection equal or better than methods such as Prewitt, Roberts, Sobel and Canny [134] do. However, it can easily be proved that all of them derive from QSA-FIT.
- In Fig.9, complementarity is shown in a symbolic way as the perfect linkage between the two theories: FFT and QSA-FIT. Instead, Fig.10 shows such complementarity and linkage in a rigorous form.

Both graphs clearly show a quadrature between FFT and FIT via equalization. FFT and FIT give information about the same physical element: frequency, but in a very different way. In fact, FIT is superior and more accurate (in its ambit) than FFT. Despite the above mentioned, both are complementary.

Thanks to these two tools (FFT and FIT) we can simultaneously get the whole universe linked to a spectral and temporal analysis of a signal, image or video. Therefore, the FFT can be indirectly located at the exact time of the signal by its components obtained thanks to FIT. This fact implies a significant advance in the Fourier's theory after almost two and a half centuries.

The above mentioned becomes much more evident when it is applied to signals as seen in the following Figures (11, 12 and 13).

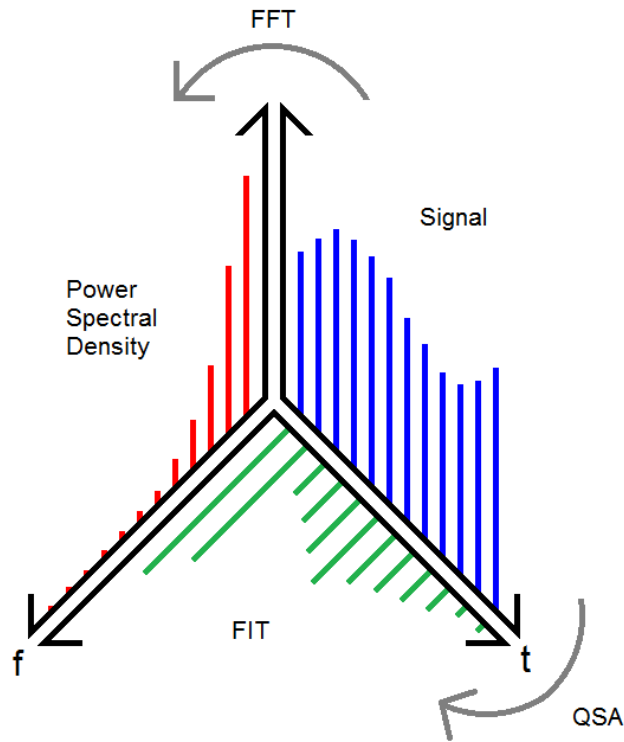


Fig.9 Symbolic relationship between FIT and FFT (PSD).

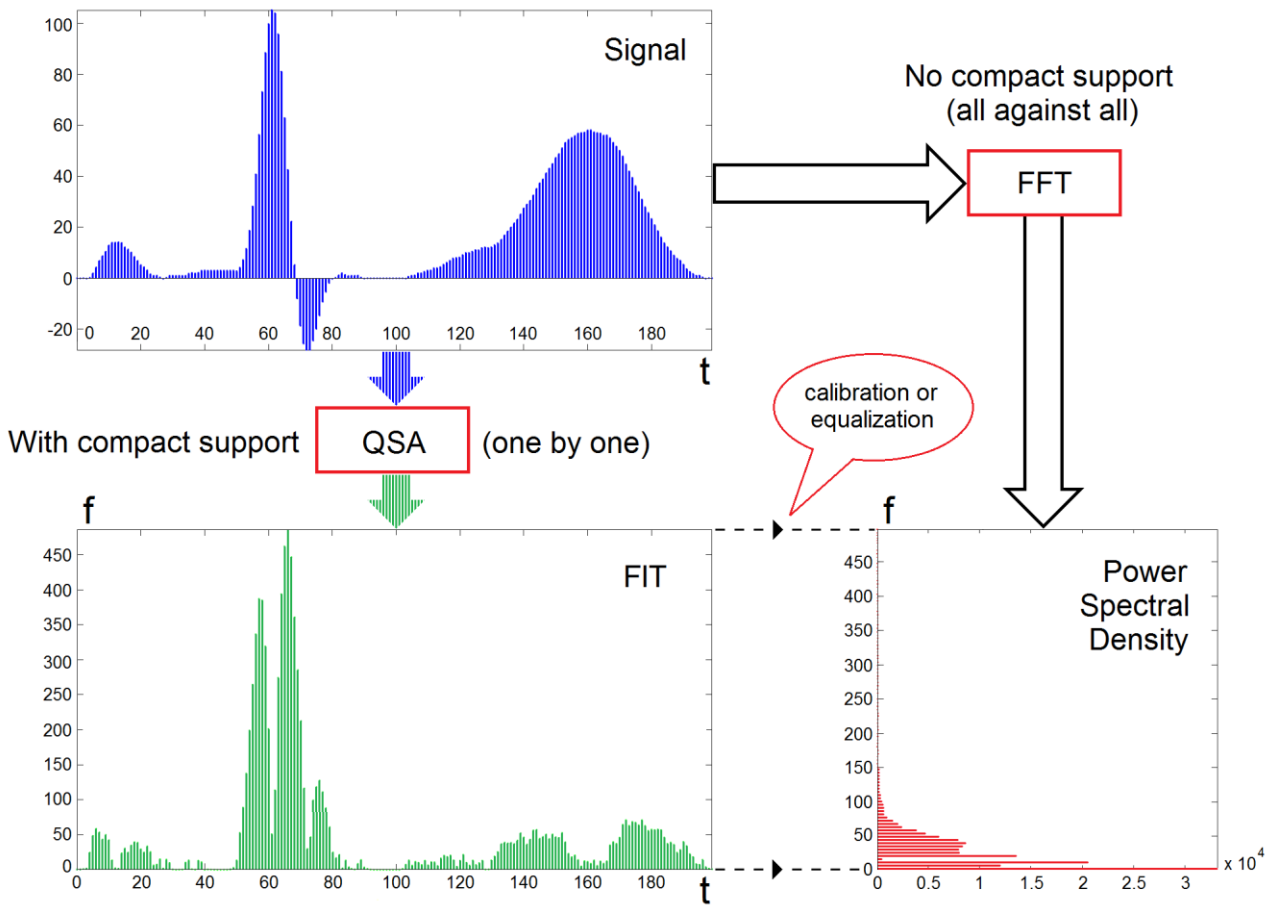


Fig.10 Rigorous relationship between FIT and FFT (PSD).

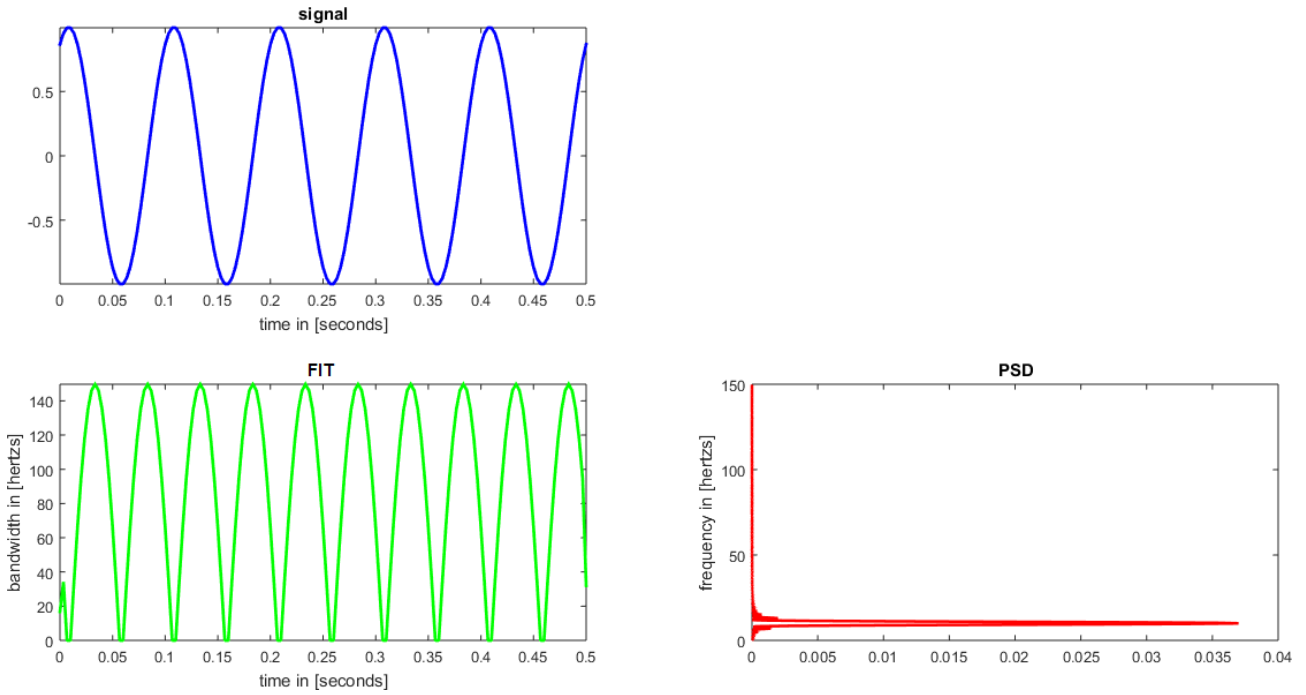


Fig.11 Original signal is a sine with a frequency of 5 Hertz.

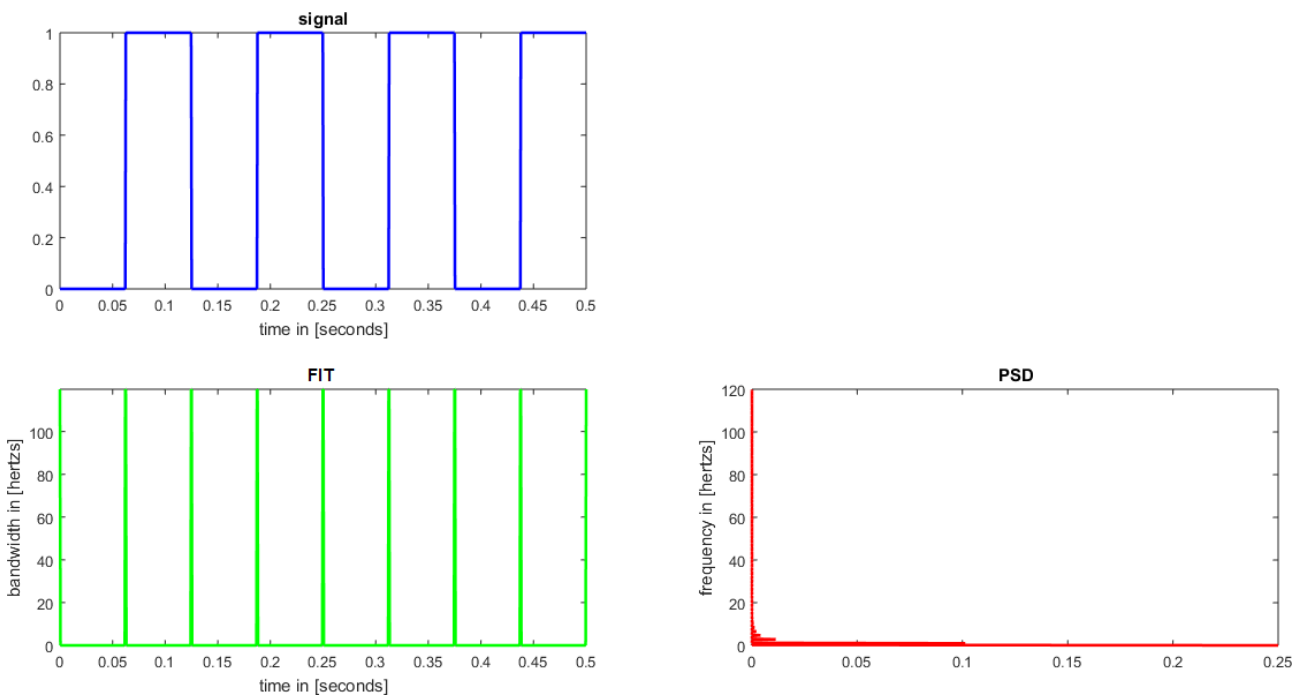


Fig.12 Original signal is a semi-gate with a frequency of 5 Hertz.

In Fig.11, a sine of 5 cycles is shown. Fig.12 depicts a train of semi-gates of 4 cycles. Finally, in Fig.13, a non-stationary signal is also viewed. Having, all of them, 1024 samples. Such figures show the coincidence between the maximum frequency of PSD with the peaks of FIT after equalization.

The most relevant aspect regarding this comparison is the fact that FFT and FIT work clearly in quadrature, representing a perfect complement among themselves, which allows to complete the indispensable toolbox required in the spectral analysis of signals, images, and videos.

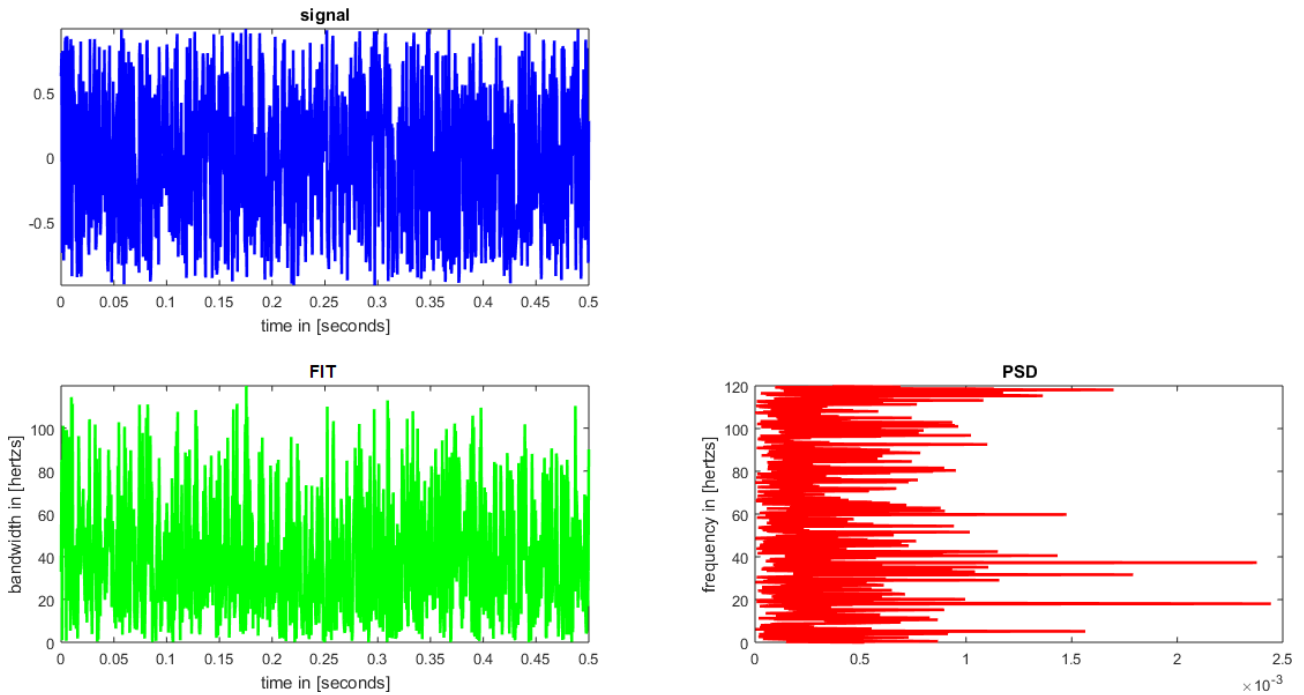


Fig.13 Original signal is a non-stationary series.

An important aspect, at this point, can be seen in Fig.12, where a semi-gate signal is discussed. The question is: why do we talk of semi-gate instead of gate directly? The answer is illustrated in Fig.14, where few samples of the semi-gate of the Fig.12 are shown in detail.

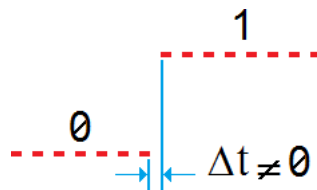


Fig.14 Some samples of Fig.12 shown in detail.

Figure 14 clearly shows the distance between two samples (in blue) of Fig.12. The latter figure represents a signal simulated in MATLAB® code:

```
% Initial parameters
f = 8; % frequency
overSampRate = 30;
fs = overSampRate*f; % sampling frequency
nCyl = 4; % number of cycles
NFFT = 1024; % number of points of FFT
nfft = NFFT/8;
t = 0:nCyl*1/f/(NFFT-1):nCyl*1/f; % time axis
x = [ zeros(1,nfft) ones(1,nfft) zeros(1,nfft) ones(1,nfft) zeros(1,nfft) ones(1,nfft) zeros(1,nfft) ones(1,nfft) ]; % signal

% Calculation of FFT
L = length(x); % length of signal
X = fftshift(fft(x,NFFT));
PSD = X.*conj(X)/(NFFT*L);
fVals = fs*(0:NFFT/2-1)/NFFT; % frequency axis
```

```

% Calculation of FIT
x_RMS = sqrt(x*x'/L);
xp = [ x(L) x x(1) ]; % padding for a cyclic signal. For a non-cyclic signal is xp = [ 0 x 0 ];
dx = [];
for n = 1:L
    dx(n) = (xp(n+2)-xp(n))/2;
end
FIT = abs(dx)/x_RMS/2/pi;
FIT = (FIT-min(FIT))/(max(FIT)-min(FIT))*(max(fVals)-min(fVals))+min(fVals);

subplot(221),plot(t,x,'b','LineWidth',2)
axis([ 0 nCyl*1/f min(x) max(x) ])
title('signal')
xlabel('time in [seconds]')

subplot(223),plot(t,FIT,'g','LineWidth',2)
axis([ 0 nCyl*1/f min(FIT) max(FIT) ])
title('FIT')
xlabel('time in [seconds]')
ylabel('frequency in [hertz]')

subplot(224),plot(PSD(NFFT/2+1:NFFT),fVals,'r','LineWidth',2)
title('PSD')
ylabel('frequency in [hertz]')

```

Figure 14 clearly shows that if $\Delta t \neq 0$, then, $\Delta\omega \neq \infty$ with $\Delta t = nCyl*1/f/(NFFT-1)$. This is the reason why we speak of semi-gate signal instead of gate. On the other hand, if we have $\Delta t = 0$, and then, $\Delta\omega = \infty$, we will speak of a gate signal.

The distribution of the witness bars is consistent with the possibility of locating a particle by its wave function, or by, the probability distribution that arises from this function.

Given the signal $y = f(t)$, the witness bars [134] arise as follows:

1. N equidistant lines are distributed along the ordinate axis, and
2. In those settings where these lines intercept the signal, we identify the projections on the axis of abscissae. On these points, we place the witness bars, which, if the signal is nonlinear, will be separated in a not equidistant way depending on the flanks of the signal at each point. This is a nonlinear sampling itself.

Some final considerations:

- The transition from QSA to FIT represents the collapse of the wave function, i.e., from vector to scalar at each moment.
- Hamiltonian is real, and, it is not hermitic for a confined single particle
- QSA-FIT can be used in time filtering
- The frequency of a pure tone (sine) is proportional to its higher slope derivative. Instead, if the signal is a gate, FIT will be infinite on the flanks, then, the density of the witness bars is infinite too in these flanks. This is very useful for a better understanding of Sampling and Nyquist theorems [139].
- Like FFT, FIT will help in the development of new algorithms for signal, image and video compression, replacing or complementing FFT or DCT in new versions of MP3 (audio [141]), JPEG (images [142]) and, H.264, H.265, VP9 and VP10 (video [143-148]).
- Unlike FFT, FIT does not require decimation in time or frequency.
- For one-dimension FFT has a computational cost of $O(N*\log_2(N))$, and FIT of $O(N)$.
- For two-dimensions FFT has a computational cost of $O(N^2*\log_2(N)^2)$, and FIT of $O(N^2)$.
- For two-dimensions FFT has a computational cost of $O(N^3*\log_2(N)^3)$, and FIT of $O(N^3)$.
- Being so simple, FIT is easily implementable in software, Field-programmable gate array (FPGA) [149], GPGPU [140], firmware [150], and Advanced RISC Machine (ARM) architecture [151].

3.4 QSA-FIT Uncertainty Principle

From Eq.(53) at each instant (without subscript by simplicity), we have,

$$\Delta\omega = \frac{1}{|S|} \frac{|\Delta S|}{\Delta t} \quad (66)$$

Then, with a simple clearance,

$$\left| \frac{\Delta S}{S} \right| = \Delta\omega \Delta t \quad (67)$$

and, if we have present Eq.(17), the equation will be,

$$\left| \frac{\Delta S}{S} \right| = \Delta\omega \Delta t \geq 1/2 \quad (68)$$

Based on Fig.15, if we define a quantum signal as a qubit sequence, and remembering Equations (21) and (22) of Section 3.1.1, spin-down is, $|\downarrow\rangle = |0\rangle$, and spin-up is $|\uparrow\rangle = |1\rangle$, then, we will have:

- *top-left*: a threshold from zero to one for a classical signal (two states)
- *top-right*: a threshold from zero to one for a classical signal (four states)
- *bottom-left*: a threshold from zero to one for a quantum signal (two states)
- *bottom-right*: a threshold from zero to one for a quantum signal (four states)

In the four cases, the flank responsible for state transition happens in an instant: $\Delta t = 0$. In fact, if we combine Eq.(15) and (66), we will have the ΔE according to QSA-FIT:

$$\Delta E = \frac{h}{|S|} \frac{|\Delta S|}{\Delta t} \quad (69)$$

Moreover, from Eq.(68) we can see a trade-off between $\Delta\omega$ and Δt , therefore, if $\Delta t = 0$, then, $\Delta\omega = \infty$, and hence, $\Delta E = \infty$. See Eq.(17), (68) and (69). The fact that $\Delta E = \infty$ does not mean that energy $E = \infty$ at all. It only means that FIT is infinite, exclusively. On the other hand, if $\Delta\omega = \infty$ (and hence, $\Delta E = \infty$) then $\Delta t = 0$. In fact, Fig.15 is an extreme case of Fig.12, with $\Delta t = 0$ and hence $\Delta\omega = \infty$. Therefore, this signal is indeed a gate.

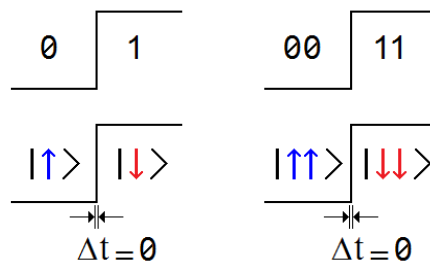


Fig.15 Flank transitions for a gate signal with $\Delta t = 0$, where, classical signals (sequence of bits) are located on the top, while, quantum signals (sequence of qubits) are on the bottom.

Now, if we apply FIT on a channel, and considering that such channel allows the survival of such type of signals with infinite frequency thanks to instantaneous transitions or flanks, then Eq.(68) can be rewritten as,

$$FRTL \geq 1/2, \quad (70)$$

where *FR* is the acronym of *frequency*, while *TL* is the acronym of *time-latency*. This means that this instantaneous change or flank generates spectral components with infinite frequency. At this point, it is necessary a better analysis of different aspects regarding the nature and origin of the channel for a deeper understanding of QSA-FIT on classical and quantum channels.

Another important concept regarding QSA-FIT is derived from Eq.(68). That equation shows the trade-off between Δt and $\Delta \omega$, through which the change in one drags the change in the other one. This also means that if $\Delta t = 0$ then $\Delta \omega = \infty$, and instead, if $\Delta \omega = \infty$, then $\Delta t = 0$. More importantly, this attribute of functional dependence is interchangeable. Since the Heisenberg Uncertainty Principle [132] exercises a strong influence over Quantum Physics, in general, and Quantum Entanglement [1-3], in particular, the projection of FIT is ensured with strong implications in Quantum Communication [152-155].

4 Conclusions and future works

This work began with an extensive tour on traditional spectral techniques based on Fourier's Theory, without the compact support and completely disconnected from the link between time and frequency (taking into consideration WT which sometimes has compact support). Besides, the responsibility of each flank with respect to final spectral components of a signal, image or video is included. For that reason QSA-FIT was created to cover such space and also as a complement to the aforementioned Fourier's Theory, in particular, FFT. A simply comparison between QSA-FIT and FFT sheds some initial conclusions, which can be seen synthesized in Table I.

When the wave function collapses, we pass from QSA to FIT. This point is essential, because it is the beginning of the necessity of using the Hadamard's quotient of vectors [57], among other practical concepts.

At this point, it is important to mention that the applications of FIT are obvious, e.g.:

- It is a support and that allows a better understanding of the Information Theory and Quantum Information Theory aimed at improving current signals, images and video compression algorithms, as well as develop new ones.
- Its applications range from filter design and signal analysis to phase retrieval and pattern recognition.
- It is an excellent complement to Spectrogram in speech processing [7, 137, 138].
- It is very useful in radar signals analysis, study of phase migration in the raw data of Synthetic Aperture Radar (SAR), Radio Astronomy, and sonar among others.
- It is particularly useful in analysis of time-varying spectral characteristics
- It represents a major contribution in Signals Intelligence (SIGINT), Imagery Intelligence (IMINT), and Communications Intelligence (COMINT) up to date.
- It retains a direct relationship with compressed sensing.
- It analysis the time series as a complement of moving average for the stock exchange.
- It analysis the biomedical signals and images including electrocardiographies, electroencephalographies, evoked potentials, and brain computer interfaces.
- It studies the seismic signals, in general, and, earthquakes, in particular.
- It studies Bioinformatics with particular emphasis in Signal Processing for DNA Sequence Analysis.
- It provides analysis, synthesis, and speech recognition.
- It is an important tool in nonlinear spectral analysis.
- It conditions acoustic spaces.
- It has applications in the study of phase in Quantum Chaos.
- Besides, its applications are obvious in a fine processing signal, namely: power spectral density (with a strict sense of time); frequency-hopping spread spectrum; analysis of stationarity; nonlinear sampling for a most efficient compression schema instead of linear sampling, among many others. See [134].

As we have already said, FIT is an extraordinary tool to assess the importance of the flanks (or edges) in a compression process weighting the importance of temporal spectral components in the final result in real time and sample by sample (or pixel by pixel).

TABLE I
COMPARISON BETWEEN FFT AND FIT

Characteristics	FFT	FIT
Separability	Yes	Yes
Compact support	No	Yes
Instantaneous spectral attributes	No	Yes
1D computational cost	$O(N \cdot \log_2(N))$	$O(N)$
2D computational cost	$O(N^2 \cdot \log_2(N)^2)$	$O(N^2)$
Energy treatment	Disastrous	Excellent
Decimation	In time or frequency	It does not require
Parallelization	No	Yes

Finally, and as we have seen, FFT does not have compact support, therefore, we say that FFT is a non-local process, while, FIT has compact support, then, FIT is a local process, with all that this means when it is applied to the study of quantum entanglement.

References

1. Nielsen, M.A., Chuang, I.L.: Quantum Computation and Quantum Information. Cambridge University Press, Cambridge (2004)
2. Kaye, P., Laflamme, R., Mosca, M.: An Introduction to Quantum Computing. Oxford University Press, Oxford (2004)
3. Stolze, J., Suter, D.: Quantum Computing: A Short Course from Theory to Experiment. WILEY-VCH Verlag GmbH & Co. KGaA, Weinheim (2007)
4. Busemeyer, J.R., Wang, Z., Townsend, J.T.: Quantum dynamics of human decision-making. *J. Math. Psychol.* **50**, 220–241 (2006) doi:10.1016/j.jmp.2006.01.003
5. Eldar, Y.C.: Quantum Signal Processing. Doctoral Thesis, MIT, Dec. 2001
6. Eldar, Y.C., Oppenheim, A.V.: Quantum Signal Processing. *Signal Process. Mag.* **19**, 12–32 (2002)
7. Vlaso, A. Y.: Quantum Computations and Images Recognition. arXiv:quant-ph/9703010 (1997)
8. Schützhold, R.: Pattern recognition on a quantum computer. *Phy. Rev. A* **67**(6), 062311 (2003)
9. Beach, G., Lomont, C., Cohen, C.: Quantum Image Processing (QuIP). *Proc. Appl. Imagery Pattern Recognit. Workshop*, 39-44 (2003)
10. Venegas-Andraca, S.E., Bose, S.: Storing, processing and retrieving an image using quantum mechanics. *Proc. SPIE Conf. Quantum Inf. Comput.* vol. 5105, 137–147 (2003)
11. Venegas-Andraca, S.E.: Discrete Quantum Walks and Quantum Image Processing. Thesis submitted for the degree of Doctor of Philosophy at the University of Oxford (2005)
12. Venegas-Andraca, S.E., Ball, J.L.: Processing images in entangled quantum systems. *Quantum Inf. Process.* **9**(1), 1-11 (2010)
13. Latorre, J.I.: Image compression and entanglement. arXiv:quant-ph/0510031 (2005)
14. Le, P.Q., Dong, F., Hirota, K.: A flexible representation of quantum images for polynomial preparation, image compression, and processing operations. *Quantum Inf. Process.* **10**(1), 63-84 (2011)
15. Sun, B., Le, P.Q., Iliyasu, A.M., *et al.*: A Multi-channel representation for images on quantum computers using the RGB color space. *Proc. IEEE 7th Intern. Symp. Intelligent Signal Proces*, 160-165 (2011)
16. Yan, F., *et al.*: Assessing the Similarity of Quantum Images based on Probability Measurements. 2012 IEEE Cong. Evolutionary Computation (CEC), 1-6 (2012)
17. Le, P.Q., Iliyasu, A.M., Dong, F., Hirota, K.: Efficient color transformations on quantum images. *J. Adv. Comput. Intell. Intell. Inf.* **15**(6), 698-706 (2011)
18. Le, P.Q., Iliyasu, A.M., Dong, F.Y., Hirota, K.: Fast Geometric Transformations on Quantum Images. *IAENG Intern. J. of Applied Mathematics.* **40**(3) (2010)
19. Le, P.Q., Iliyasu, A.M., Dong, F.Y., Hirota, K.: Strategies for designing geometric transformations on quantum images. *Theoretical Computer Science.* **412**(15), 1506-1418 (2011)
20. Srivastava, M., Panigrahy, P.K.: Quantum Image Representation Through Two-Dimensional Quantum States and Normalized Amplitude. arXiv:quant-ph/1305.2251 (2013)

21. Li, H.S., Zhu, Q.X., Lan, S., *et al.*: Image storage, retrieval, compression and segmentation in a quantum system. *Quantum Inf. Process.* **12**(6), 2269-2290 (2013)
22. Li, H.S., Zhu, Q.X., Li, M.C., *et al.*: Multidimensional color image storage, retrieval, and compression based on quantum amplitudes and phases. *Information Sciences.* **273**, 212-232 (2014)
23. Hu, B.Q., Huang, X.D., Zhou, R.G. *et al.*: A theoretical framework for quantum image representation and data loading scheme *Science China on Information Science.* **57**(3),1-11 (2014)
24. Zhang, Y., Lu, K., Gao, Y., Wang, M.: NEQR: a novel enhanced quantum representation of digital images. *Quantum Inf. Process.* **12**(8), 2833-2860 (2013)
25. Wang, M., Lu, K., Zhang, Y.: FLPI: representation of quantum images for log-polar coordinate. *Fifth Intern. Conf. on Digital Image Processing: ICDIP'2013* (2013)
26. Zhang, Y., Lu, K., Gao, Y., Wang, M.: A novel quantum representation for log-polar images. *Quantum Inf. Process.* **12**(8), 3103-3126 (2013)
27. Yuan, S., Mao, X., Chen, L. *et al.*: Quantum digital image processing algorithms based on quantum measurement. *Optik - International Journal for Light and Electron Optics.* **124**(23), 6386-6390 (2013)
28. Yuan, S., Mao, X., Xue, Y., *et al.*: SQR: a simple quantum representation of infrared images. *Quantum Inf. Process.* **13**(6), 1353-1379 (2014)
29. Zhang, W.W., Gao, F., Liu B.: A quantum watermark protocol. *Int. J. Theor. Phys.* **52**(2), 504-513 (2013)
30. Zhang, W.W., Gao, F., Liu B., *et al.*: A watermark strategy for quantum images based on quantum fourier transform. *Quantum Inf. Process.* **12**(2), 793-803 (2013)
31. Yang, Y.G., Xia, J., Jia, X., *et al.*: Novel image encryption/decryption based on quantum Fourier transform and double phase encoding. *Quantum Inf. Process.* **12**(11), 3477-3493 (2013)
32. Yang, Y.G., Jia, X., Sun, S.J., *et al.*: Quantum cryptographic algorithm for color images using quantum Fourier transform and double random-phase encoding. *Information Sciences.* **277**, 445-457 (2014)
33. Song, X.H., Niu, X.M.: Comment on: Novel image encryption/decryption based on quantum fourier transform and double phase encoding. *Quantum Inf. Process.* **13**(6), 1301-1304 (2014)
34. Jiang, N., Wu, W.Y., Wang, L.: The quantum realization of Arnold and Fibonacci image scrambling *Quantum Information Processing.* *Quantum Inf. Process.* **13**(5), 1223-1236 (2014)
35. Zhou, R.G., Wu, Q., Zhang, M.Q., Shen, C.Y.: Quantum image encryption and decryption algorithms based on quantum image geometric transformations. *Int. J. Theor. Phys.* **52**(6), 1802-1817 (2013)
36. Tseng, C.C., Hwang, T.M.: *Quantum Digital Image Processing Algorithms.* 16th IPPR Conf. on Computer Vision, Graphics and Image Processing: CVGIP'2003. Kinmen, Taiwan (2003)
37. Mastriani, M.: *Quantum Image Processing?* *Quantum Inf Process* (2017) 16:27. doi:10.1007/s11128-016-1457-y
38. Altepeter, J.B., Branning, D., Jeffrey, E., Wei, T.C., Kwiat, P.G., Thew, R.T., O'Brien, J.L., Nielsen, M.A., White, A.G.: Ancilla-assisted quantum process tomography. *Phys. Rev. Lett.* **90**, 193601 (2003)
39. Niggebaum, A.: *Quantum State Tomography of the 6 qubit photonic symmetric Dicke State.* Thesis submitted for the degree of Doctor of Physics. Ludwig-Maximilians-Universität München (2011)
40. Gross, D., Liu, Y.-K., Flammia, S.T., Becker, S., Eisert, J.: Quantum state tomography via compressed sensing. arXiv:0909.3304 [quant-ph] (2010)
41. Audenaert, K.M.R., Scheel, S.: Quantum tomographic reconstruction with error bars: a Kalman filter approach. *N. J. Phys.* **11**, 023028 (2009)
42. Jain, A.K.: *Fundamentals of Digital Image Processing.* Prentice Hall Inc., Englewood Cliffs, NJ (1989)
43. Gonzalez, R.C., Woods, R.E.: *Digital Image Processing,* Prentice-Hall, Englewood Cliffs (2002)
44. Gonzalez, R.C., Woods, R.E., Eddins, S.L.: *Digital Image Processing Using Matlab.* Pearson Prentice Hall, Upper Saddle River (2004)
45. Schalkoff, R.J.: *Digital Image Processing and Computer Vision.* Wiley, New York (1989)
46. MATLAB® R2015a (Mathworks, Natick, MA). <http://www.mathworks.com/>
47. Mastriani, M.: Quantum Boolean image denoising. *Springer Quantum Information Processing.* **14**(5), 1647-1673 (2015)
48. Weinstein, Y.S., Lloyd, S., Cory, D.G.: Implementation of the Quantum Fourier Transform (1999) quant-ph arXiv:quant-ph/9906059v1
49. Wikipedia. https://en.wikipedia.org/wiki/Fourier_transform
50. Hsu, H.P.: *Fourier Analysis.* Simon & Schuster, New York (1970)
51. Wikipedia. https://en.wikipedia.org/wiki/Discrete_Fourier_transform

52. Tolimieri R., An M., Lu C.: Algorithms for Discrete Fourier Transform and convolution. Springer Verlag, New York (1997)
53. Tolimieri R., An M., Lu C.: Mathematics of multidimensional Fourier Transform Algorithms. Springer Verlag, New York (1997)
54. Briggs, W.L., Van Emden, H.: The DFT: An Owner's Manual for the Discrete Fourier Transform. SIAM, Philadelphia (1995)
55. Oppenheim, A.V, Willsky, A.S., Nawab, S. H.: Signals and Systems. Second Edition, Prentice Hall, Upper Saddle River, NJ (1997)
56. Oppenheim, A.V, Schafer, R.W.: Digital Signal Processing. Prentice Hall, Englewood Cliffs, NJ (1975)
57. De Graeve, R., Parisse, B.: Symbolic algebra and Mathematics with Xcas. University of Grenoble I (2007) https://www-fourier.ujf-grenoble.fr/~parisse/giac/cascmd_en.pdf
58. Wikipedia. https://en.wikipedia.org/wiki/Fast_Fourier_transform
59. Van Loan, C.: Computational Frameworks for the Fast Fourier Transform, SIAM (1992)
60. Heideman, M.T., Johnson, D.H., Burrus, C.S.: Gauss and the history of the fast Fourier transform. IEEE ASSP Magazine 1(4), 14–21 (1984) doi:10.1109/MASSP.1984.1162257
61. Strang, G.: Wavelets. American Scientist 82(3), 253 (1994)
62. Dongarra, J., Sullivan, F: Guest Editors Introduction to the top 10 algorithms. Computing in Science Engineering 2(1), 22–23 (2000) doi:10.1109/MCISE.2000.814652. ISSN 1521-9615
63. Wikipedia. https://en.wikipedia.org/wiki/Short-time_Fourier_transform
64. Sejdić, E., Djurović, I., Jiang, J.: Time-frequency feature representation using energy concentration: An overview of recent advances. Digital Signal Processing. 19(1), 153-183 (2009)
65. Jacobsen, E., Lyons, R.: The sliding DFT. Signal Processing Magazine. 20(2), 74–80 (2003)
66. Allen, J.B.: Short Time Spectral Analysis, Synthesis, and Modification by Discrete Fourier Transform. IEEE Trans. on Acoustics, Speech, and Signal Processing. ASSP-25 (3), 235–238 (1977)
67. https://en.wikipedia.org/wiki/Gabor_transform
68. Wikipedia. https://en.wikipedia.org/wiki/Fractional_Fourier_transform
69. Condon, E.U.: Immersion of the Fourier transform in a continuous group of functional transformations. *Proc. Nat. Acad. Sci. USA* **23**, 158–164 (1937)
70. Namias, V.: The fractional order Fourier transform and its application to quantum mechanics. *J. Inst. Appl. Math.* **25**, 241–265 (1980)
71. Wiener, N.: Hermitian Polynomials and Fourier Analysis. *J. Mathematics and Physics* **8**, 70-73 (1929)
72. Almeida, L.B.: The fractional Fourier transform and time-frequency representations. *IEEE Trans. Sig. Processing* **42**(11), 3084–3091 (1994)
73. Tao, R., Deng, B., Zhang, W.-Q, Wang, Y.: Sampling and sampling rate conversion of band limited signals in the fractional Fourier transform domain. *IEEE Trans. on Signal Processing*, **56**(1), 158–171 (2008)
74. Bhandari, A., Marziliano, P.: Sampling and reconstruction of sparse signals in fractional Fourier domain. *IEEE Signal Processing Letters*, **17**(3), 221–224 (2010)
75. Bailey, D.H., Swartztrauber, P.N.: The fractional Fourier transform and applications. *SIAM Review* **33**, 389-404 (1991)
76. Shi, J., Zhang, N.-T., Liu, X.-P.: A novel fractional wavelet transform and its applications. *Sci. China Inf. Sci.* **55**(6), 1270-1279 (2012)
77. De Bie, H.: Fourier transform and related integral transforms in superspace. (2008) <http://www.arxiv.org/abs/0805.1918>
78. Fan, H.-Y., Hu, L.-Y.: Optical transformation from chirplet to fractional Fourier transformation kernel (2009) <http://www.arxiv.org/abs/0902.1800>
79. Klappenecker, A., Roetteler, M.: Engineering Functional Quantum Algorithms (2002) <http://www.arxiv.org/abs/quant-ph/0208130>
80. Sejdić, E., Djurović, I., Stanković, L.J.: Fractional Fourier transform as a signal processing tool: An overview of recent developments. *Signal Processing*. 91(6), 1351-1369 (2011)
81. Pégard, N.C., Fleischer, J.W.: Optimizing holographic data storage using a fractional Fourier transform. *Opt. Lett.* **36**, 2551-2553 (2011)
82. Ding, J.J.: Time frequency analysis and wavelet transform class note, the Department of Electrical Engineering, National Taiwan University (NTU), Taipei, Taiwan (2007)
83. Wikipedia. https://en.wikipedia.org/wiki/Wavelet_transform

84. Meyer, Y.: *Wavelets and Operators*. Cambridge: Cambridge University Press. (1992)
85. Chui, C.K.: *An Introduction to Wavelets*. San Diego: Academic Press. (1992)
86. Akansu, A.N., Haddad, R.A.: *Multiresolution Signal Decomposition: Transforms, Subbands, Wavelets*. San Diego: Academic Press. (1992)
87. Wikipedia. https://en.wikipedia.org/wiki/JPEG_2000
88. Malmurugan, N., Shanmugam, A., Jayaraman, S., Chander, V.V.D.: A New and Novel Image Compression Algorithm Using Wavelet Footprints. *Academic Open Internet Journal*. 14 (2005)
89. Ho, T.W., Jeoti, V.: A wavelet footprints-based compression scheme for ECG signals. *IEEE Region 10 Conference TENCON 2004*. A., 283. (2004) doi:10.1109/TENCON.2004.1414412
90. Krantz, S.G.: *A Panorama of Harmonic Analysis*. Mathematical Association of America. (1999)
91. Drozdov, A.: Comparison of wavelet transform and fourier transform applied to analysis of non-stationary processes. *Nanosystems: physics, chemistry, mathematics* **5**: 363–373. (2014)
92. Martin, E.: Novel method for stride length estimation with body area network accelerometers. *IEEE BioWireless 2011*, Univ. of California, Berkeley, CA, USA, 79-82 (2011)
93. Liu, J.: Shannon wavelet spectrum analysis on truncated vibration signals for machine incipient fault detection. *Measurement Science and Technology* **23** (5): 1–11 (2012) doi:10.1088/0957-0233/23/5/055604
94. Akansu, A.N., Serdijn, W.A., Selesnick, I.W.: Emerging applications of wavelets: A review. *Physical Communication* **3**: 1. (2010) doi:10.1016/j.phycom.2009.07.001
95. Donoho, D.L.: De-noising by soft-thresholding. *IEEE Trans. Inform. Theory*. **41**(3), 613-627 (1995)
96. Donoho, D.L., Johnstone, I.M.: Adapting to unknown smoothness via wavelet shrinkage. *Journal of the American Statistical Assoc.* **90**(432), 1200-1224 (1995)
97. Donoho, D.L., Johnstone, I.M.: Ideal spatial adaptation by wavelet shrinkage. *Biometrika*. 81, 425-455 (1994)
98. Daubechies, I.: *Ten Lectures on Wavelets*. SIAM, Philadelphia, PA (1992)
99. Daubechies, I.: *Different Perspectives on Wavelets*. Proceedings of Symposia in Applied Mathematics, vol. 47, American Mathematical Society, USA (1993)
100. Mallat, S.G.: A theory for multiresolution signal decomposition: The wavelet representation. *IEEE Trans. Pattern Anal. Machine Intell.* **11**(7), 674–693 (1989)
101. Mallat, S.G.: Multiresolution approximations and wavelet orthonormal bases of $L_2(\mathbb{R})$. *Transactions of the American Mathematical Society*, **315**(1), 69-87 (1989)
102. Zhang, X.-P., Desai, M.: Nonlinear adaptive noise suppression based on wavelet transform. *Proceedings of the ICASSP98*, vol. 3, 1589-1592, Seattle (1998)
103. Zhang, X.-P.: Thresholding Neural Network for Adaptive Noise reduction. *IEEE Transactions on Neural Networks*. **12**(3), 567-584 (2001)
104. Zhang, X.-P., Desai, M.: Adaptive Denoising Based On SURE Risk. *IEEE Signal Proc. Letters*. **5**(10), 265-267 (1998)
105. Zhang, X.-P., Luo, Z.Q.: A new time-scale adaptive denoising method based on wavelet shrinkage. *Proceedings of the ICASSP99*, Phoenix, AZ., March 15-19 (1999)
106. Lang, M., Guo, H., Odegard, J., Burrus, C., Wells, R.: Noise reduction using an undecimated discrete wavelet transform. *IEEE Signal Proc. Letters*, **3**(1), 10-12 (1996)
107. Chipman, H., Kolaczyk, E., McCulloch, R.: Adaptive Bayesian wavelet shrinkage. *J. Amer. Statist. Assoc.* 92, 1413–1421 (1997)
108. Chang, S.G., Yu, B., Vetterli, M.: Spatially adaptive wavelet thresholding with context modeling for image denoising. *IEEE Trans. Image Processing*. **9**(9), 1522–1531 (2000)
109. Chang, S.G., Yu, B., Vetterli, M.: Adaptive wavelet thresholding for image denoising and compression. *IEEE Trans. Image Processing*. **9**(9), 1532–1546 (2000)
110. Chang, S.G., Vetterli, M.: Spatial adaptive wavelet thresholding for image denoising. *Proc. ICIP*. vol. 1, 374–377 (1997)
111. Crouse, M.S., Nowak, R.D., Baraniuk, R.G.: Wavelet-based statistical signal processing using hidden Markov models. *IEEE Trans. Signal Processing*. **46**(4), 886–902 (1998)
112. Malfait, M., Roose, D.: Wavelet-based image denoising using a Markov random field *a priori* model. *IEEE Trans. Image Processing*. **6**(4), 549–565 (1997)
113. Mihcak, M.K., Kozintsev, I., Ramchandran, K., Moulin, P.: Low complexity image denoising based on statistical modeling of wavelet coefficients. *IEEE Trans. Signal Processing Lett.* **6**(12), 300–303 (1999)

114. Simoncelli, E.P.: Bayesian denoising of visual images in the wavelet domain. *Bayesian Inference in Wavelet Based Models*. New York: Springer-Verlag, pp. 291–308 (1999)
115. Simoncelli, E., Adelson, E.: Noise removal via Bayesian wavelet coring. *Proc. ICIP*, vol. 1, pp. 379–382 (1996)
116. Belge, M., Kilmer, M.E., Miller, E.L.: Wavelet domain image restoration with adaptive edge-preserving regularization. *IEEE Trans. Image Processing*. **9**(4), 597–608 (2000)
117. Liu, J., Moulin, P.: Information-theoretic analysis of interscale and intrascale dependencies between image wavelet coefficients. *IEEE Trans. Image Processing*. **10**(11), 1647–1658 (2000)
118. Guo, H., Odegard, J.E., Lang, M., Gopinath, R.A., Selesnick, I., Burrus, C.S.: Speckle reduction via wavelet shrinkage with application to SAR based ATD/R. Technical Report CML TR94-02, CML, Rice University, Houston (1994)
119. Coifman, R.R., Donoho, D.L.: Translation-invariant de-noising. A. Antoniadis & G. Oppenheim (eds), *Lecture Notes in Statistics*. Springer-Verlag. vol. 103, pp 125-150 (1995)
120. Misiti, M., Misiti, Y., Oppenheim, G., Poggi, J.M.: *Wavelet Toolbox, for use with MATLAB®, User's guide, R2015b* (2015) http://www.mathworks.com/help/pdf_doc/wavelet/wavelet Ug.pdf
121. Burrus, C.S., Gopinath, R.A., Guo, H.: *Introduction to Wavelets and Wavelet Transforms: A Primer*. Prentice Hall, New Jersey (1998)
122. Hubbard, B.B.: *The World According to Wavelets: The Story of a Mathematical Technique in the Making*. A. K. Peter Wellesley Eds., Massachusetts (1996)
123. Grossman, A., Morlet, J.: Decomposition of Hardy Functions into Square Integrable Wavelets of Constant Shape. *SIAM J. App Math*. vol. 15, 723-736 (1984)
124. Valens, C.: A really friendly guide to wavelets (2004) <http://perso.wanadoo.fr/polyvalens/clemens/wavelets/wavelets.html>
125. Kaiser, G.: *A Friendly Guide To Wavelets*. Boston: Birkhauser (1994)
126. Walker, J.S.: *A Primer on Wavelets and their Scientific Applications*. Chapman & Hall/CRC, New York (1999)
127. Stollnitz, E.J., DeRose, T.D., Salesin, D.H.: *Wavelets for Computer Graphics: Theory and Applications*. Morgan Kaufmann Publishers, San Francisco (1996)
128. Shen, J., Strang, G.: The zeros of the Daubechies polynomials. *Proc. American Mathematical Society* (1996)
129. Yu, R., Allen, A.R., Watson, J.: An optimal wavelet thresholding for speckle noise reduction. *Summer School on Wavelets: Papers*, Publisher: Silesian Technical University, Gliwice, Poland. 77-81 (1996)
130. Gao, H.Y., Bruce, A.G.: WaveShrink with firm shrinkage. *Statistica Sinica*. 7, 855-874 (1997)
131. Gagnon, L., Smaili, F.D.: Speckle noise reduction of airborne SAR images with Symmetric Daubechies Wavelets. *SPIE Proc.* #2759. 14-24 (1996).
132. Wikipedia. https://en.wikipedia.org/wiki/Uncertainty_principle
133. Wikipedia. https://en.wikipedia.org/wiki/Root_mean_square
134. Mastriani, M.: *Quantum spectral analysis: frequency in time with applications to signal and image processing* (2017) <hal-01654125>
135. Oppenheim, A.V., Willsky, A.S., and, Nawab, S.H.: *Signals and Systems, Second Edition*. Upper Saddle River, NJ: Prentice-Hall, Inc. (1997)
136. Briggs, W.L., and, Van Emden H.: *The DFT: An Owner's Manual for the Discrete Fourier Transform*, SIAM, Philadelphia (1995)
137. Oppenheim, A.V., and, Schafer, R.W.: *Discrete-Time Signal Processing, Third Edition*. Upper Saddle River, NJ: Prentice-Hall, Inc. (2010)
138. Oppenheim, A.V., and, Schafer, R.W., and, Buck, J.R.: *Discrete-Time Signal Processing, Second Edition*. Upper Saddle River, NJ: Prentice-Hall, Inc. (1999)
139. Gonorovski, I.S.: *Radio circuits and signals*. MIR Publishers, Moscow (1986)
140. NVIDIA® Tesla® 2050 GPU. <http://www.nvidia.com/>
141. <https://en.wikipedia.org/wiki/MP3>
142. Miano, J.: *Compressed image file formats: JPEG, PNG, GIF, XBM, BMP*. ACM Press/Addison-Wesley Publishing Co. New York, NY, USA (1999)
143. Wien, M.: *Variable Block-Size Transforms for Hybrid Video Coding*, Degree Thesis, Institut für Nachrichtentechnik der Rheinisch-Westfälischen Technischen Hochschule Aachen, February 2004.
144. https://en.wikipedia.org/wiki/Video_codec

145. <https://en.wikipedia.org/wiki/VP9>
146. <https://en.wikipedia.org/wiki/VP9#VP10>
147. https://en.wikipedia.org/wiki/H.264/MPEG-4_AVC
148. https://en.wikipedia.org/wiki/High_Efficiency_Video_Coding
149. https://en.wikipedia.org/wiki/Field-programmable_gate_array
150. <https://en.wikipedia.org/wiki/Firmware>
151. https://en.wikipedia.org/wiki/ARM_architecture
152. Cariolaro, G.: Quantum Communications. Springer International Publishing (2015)
153. Mishra, V.K.: An Introduction to Quantum Communication. Momentum Press (2016)
154. Imre, S., Gyongyosi, L.: Advanced Quantum Communications: An Engineering Approach. Wiley-IEEE Press (2012)
155. NIST: Quantum Computing and Communication. CreateSpace Independent Publishing Platform (2014)